Commonality and Variability in Functional Networks In Young Children Under 5 Years Old

Jiaxin Cindy Tu[1,2], Chenyan Lu[1], Trevor K. M. Day[3,4,5], Robert Hermosillo[3], Lucille A. Moore[3], Anxu Wang[1], Xintian Wang[1], Donna Dierker[1], Aidan Latham[6], Jeanette K. Kenley[6], Damien A. Fair[3,4], Jed T. Elison[3,4], Chad M. Sylvester[1,8,10], Barbara B. Warner[7], Joan L. Luby[8], Cynthia E. Rogers[8], Deanna M. Barch[1,8,9], Christopher D. Smyser[1,6,7,8], Timothy O. Laumann[8], Evan M. Gordon[1], Adam T. Eggebrecht[1], Muriah D. Wheelock[1]

[1]Mallinckrodt Institute of Radiology, Washington University in St. Louis, USA. [2]Department of Psychological and Brain Sciences, Dartmouth College, USA.[3]Masonic Institute for the Developing Brain, University of Minnesota, USA. [4]Institute of Child Development, University of Minnesota, USA. [5]Center for Brain Plasticity and Recovery, Georgetown University, USA. [6]Department of Neurology, Washington University in St. Louis, USA. [7]Department of Pediatrics, Washington University in St. Louis, USA. [8]Department of Psychiatry, Washington University in St. Louis, USA. [9]Department of Psychological and Brain Sciences, Washington University in St. Louis, USA. [10]The Taylor Family Institute for Innovative Psychiatric Research, Washington University in St. Louis, USA.

Corresponding Author
Muriah Wheelock
Mallinckrodt Institute of Radiology
4525 Scott Ave
St. Louis, MO 63110
mdwheelock@wustl.edu

Abstract

Functional brain networks exhibit striking individual variability in adults, while less is known about the functional network variability in young children under 5 years. Conventional group-average approaches to obtain the group-level network may have obscured some fine developmental details. We combined data-driven template creation at a coarse parcel level and template-matching at a fine vertex level to map individualized functional networks from single fMRI scans in children aged 8-60 months in two datasets, revealing four key insights: (1) Individual-specific networks show moderate stability across longitudinal scans (Normalized Mutual Information ~ 0.52 with ~ 20 minutes of low-motion data) despite developmental changes; (2) Across the population, sensory cortices demonstrate higher consistency in network assignment than association cortices; (3) Network lateralization in the language network increases with age and correlates with age-normalized verbal developmental quotient (r ~ 0.17), suggesting a correspondence between the individual functional topography and the emergence of functional specialization; and (4) Our 23-network solution identifies finer subdivisions than previously reported using group-average approaches, with many networks resembling the subdivisions found in adult fMRI data. Our findings revealed neurodevelopmental variations in functional network topography that are reliable within individuals and behaviorally relevant, opening new avenues for investigating how person-specific network architecture supports emerging cognitive abilities.

Introduction

Functional network patterns in young children (< 5 years) have been characterized at the group level (Eggebrecht et al., 2017; Kardan et al., 2022; Myers et al., 2024; Sylvester et al., 2022; Tu et al., 2025a; Wang et al., 2023). However, these group-average pediatric brain networks may not comprehensively represent the organization of the developing brain. Recent studies in adults have demonstrated idiosyncratic yet reliable features in functional network topography across individuals that are qualitatively different from group-average estimates

(Bijsterbosch et al., 2023; Braga and Buckner, 2017; Dworetsky et al., 2021; Gordon et al., 2017c, 2017b; Gratton et al., 2018; Laumann et al., 2015). These trait-like topographical features are stable across both sessions (Seitzman et al., 2019) and task states (Kraus et al., 2021), and may be related to individual behavioral characteristics (Cui et al., 2020) or clinical phenotypes (Lynch et al., 2024). Group-averaging procedures not only fail to capture these individual-specific features, but they also tend to obscure networks with highly variable spatial topographies across individuals (Ladwig et al., 2025). Therefore, we reasoned that using an approach that circumvents the group-averaging could potentially reveal finer network details in a pediatric population, which may reveal unique developmental changes and variability.

Reliable identification of individual-specific functional networks with unsupervised clustering/community detection techniques often requires extended data acquisition. For example, with the commonly used Infomap algorithm (Power et al., 2011; Rosvall and Bergstrom, 2008), more than 90-100 minutes of data has been recommended (Gordon et al., 2017c; Laumann et al., 2015). However, starting these analyses de novo for every new individual might not be necessary, given that most resting-state functional network topography is consistent across individuals (Damoiseaux et al., 2006; Dworetsky et al., 2021; Gratton et al., 2018). Consequently, several prior-based methods have been developed to derive individual-specific functional networks in populations with limited data available per individual (Gordon et al., 2017a; Hacker et al., 2013; Hermosillo et al., 2024; Kong et al., 2019; Li et al., 2019; Luckett et al., 2023; Wang et al., 2015), significantly lowering the data requirement (Hermosillo et al., 2024; Kong et al., 2019).

Although the aforementioned prior-based methods have significantly advanced the mapping of individual-specific network organizations, the selection of network priors remains a critical decision that has been frequently overlooked, especially when applying these methods to populations beyond healthy, young adults. For example, previous work has used a set of adult network priors for data acquired in children younger than 5 years old (Moore et al., 2024; Sun et al., 2025), which assumes that the number and spatial topography of functional networks in pediatric cohorts are reasonably similar to the adult population average. However, mounting evidence suggests functional connectivity (FC) and network features in young children consistently differ from older children and adults (Eggebrecht et al., 2017; Fransson et al., 2007; Gao et al., 2015a, 2015b; Kardan et al., 2022; Marrus et al., 2018; Myers et al., 2024; Sylvester et al., 2022; Tu et al., 2025a, 2025b; Wang et al., 2023). Notably, while some studies have proposed deriving infant-specific network templates by averaging BOLD time series at cortical locations defined by adult networks to calculate network-average FC profiles (Moore et al., 2024), it remains unclear whether this approach necessarily yields truly “age-specific” networks. To date, few studies have delineated individual-specific networks in children younger than 5 years old using age-specific group priors (Derman et al., 2025).

Additionally, hemispheric lateralization of functional networks has been consistently observed in prior literature, especially in heteromodal association cortices (Wang et al., 2014, 2015; Perez et al., 2023). For example, the language network exhibits a left-hemisphere bias (Braga et al., 2020; Lipkin et al., 2022; Wang et al., 2015), while the ventral attention network shows a right-hemisphere bias (Bernard et al., 2020; Wang et al., 2015). Furthermore, left lateralization in the language network strengthens from childhood into young adulthood (Holland et al., 2007; Lidzba et al., 2011; Olulade et al., 2020; Sepeta et al., 2016; Szaflarski et al., 2006b, 2006a), with individual differences in network lateralization linked to handedness (Perez et al., 2023; Wang et al., 2015). However, it is unclear how early hemispheric lateralization emerges in young children and whether it is associated with the development of behavioral functions such as language.

Here, we demonstrate functional network organization variations across both individuals and chronological age in children at 1 to 5 years old using two datasets and fine network divisions representative in young children. Specifically, we first identified group-level network

templates using high-quality scan sessions with >20 minutes of low-motion data at 2 and 3 years and then created vertex-level individual-specific networks using fMRI data from a single scan session. This approach enabled inclusion of network details not previously described in group data in this age range and provided a prior for noise-robust subject-specific network localization. Our analyses shows that using age-specific network priors supports individual-specific network organizations can be determined using 10-20 minutes of low-motion fMRI data in young children. The population consensus assignment from individual network maps produced a cleaner and finer group-level division than networks found on group-average FC data. Furthermore, lateralization in the language network increased with age, with greater lateralization positively associated with age-normalized verbal developmental quotient. Taken together, our results offer insights into commonality and variability in functional network topography in young children before 5 years and provide insights into functional specialization in the developing brain.

Results

Building a representative group network template through clustering concatenated individuals' FC data

Previously, we identified functional networks based on group-average FC in 2-year-olds using an age-specific area parcellation (Tu et al., 2025a). However, due to individual variability, anatomically matched areas from different individuals may possess distinct FC profiles. Thus, group averaging could obscure finer individual-specific features present in individual participants' data (Supplementary Figure 1, details in Supplementary Text). In contrast, to prevent the smoothing effect of group-averaging, one could also concatenate FC matrices across individuals (using the same area parcellation (Tu et al., 2025a)) and look for common FC patterns across both seed area and participants. Specifically, we concatenated and clustered the FC from 81 fMRI sessions (from 72 unique participants, including 9 participants with 2 longitudinal sessions at both Y2 and Y3, each with >20 minutes of low-motion data from a group of 2-3 year-olds in the eLABE dataset, Dataset 1, Supplementary Figure 2). FC from these "template sessions" were clustered using a K-means clustering algorithm (Figure 1A), analogous to prior literature (Yeo et al., 2011; Zhu et al., 2025). We identified a local peak of stability at K = 23 clusters using a split-half stability analysis (Supplementary Figure 3). A description of this procedure is provided in Materials and Methods.

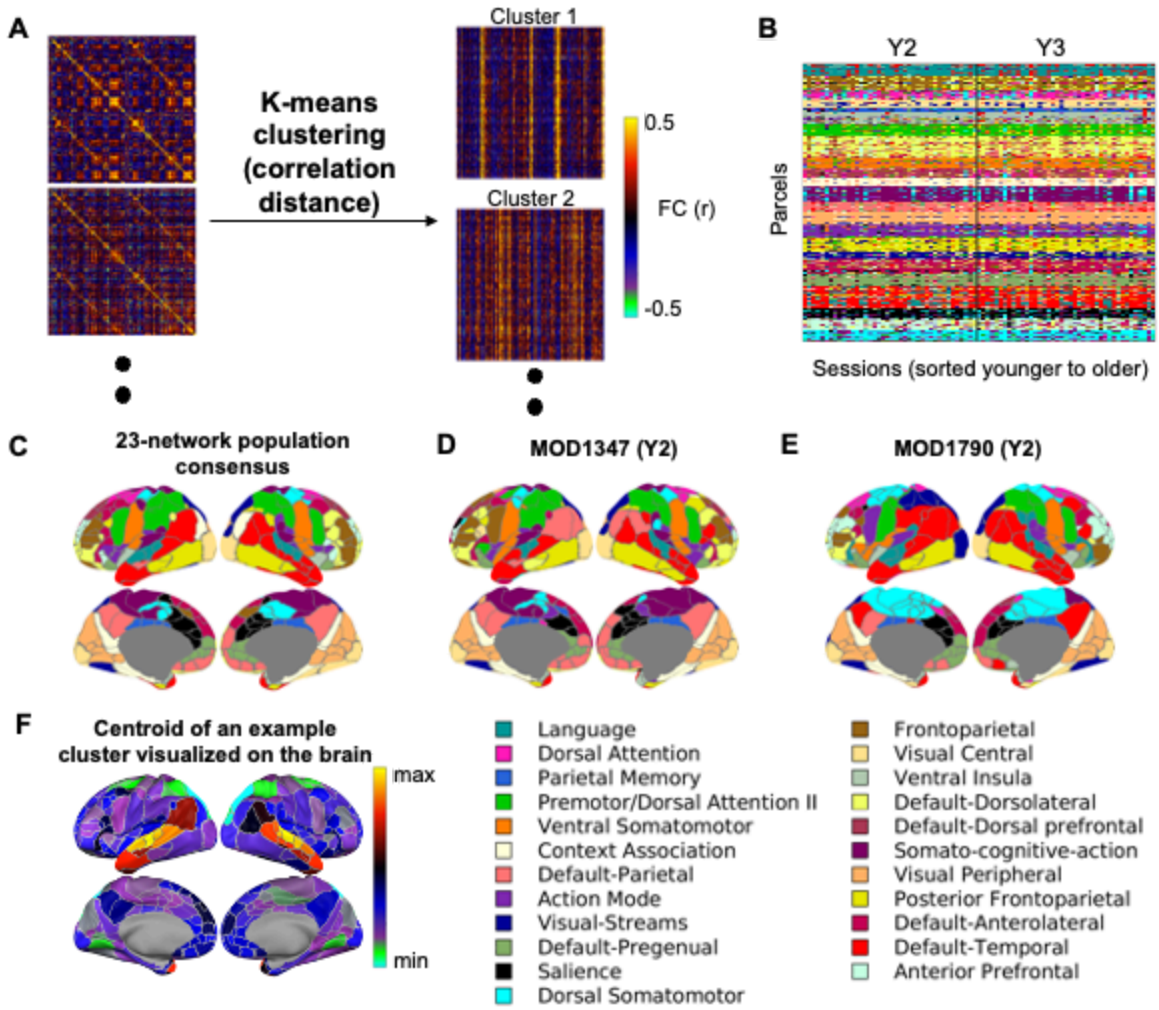

Figure 1. *K-means clustering on concatenated FC profiles using an age-specific area parcellation for young children.* A) Example FC matrices were concatenated and clustered into internally similar clusters of FC profiles. B) Network assignment across sessions for the 23-network solution. Y2/Y3 are the two-year and 3-year time points of the eLABE dataset collected at around 2 years and 3 years after birth, respectively. C) The population consensus (most frequent assignment across individuals) of the 23-network solution. D-E) Network assignments for two example sessions. F) Example template FC profiles (centroids) for the Language network.

The 23 resting-state network profiles produced by this procedure are the representative FC profiles in the group. As expected, these networks were present in similar sets of area parcels across 81 sessions (Figure 1B). This pattern is also evident when comparing the population consensus, i.e. most frequent network assignments (Figure 1C) with the individual sessions (e.g., Figure 1D-E). The centroids of the clusters can now be used as "network templates" (one example in Figure 1F; all 23 networks in Supplementary Figure 4). The functional connectivity profile from each vertex to all parcels (vertex-to-parcel connectivity map) were compared with all 23 network templates using Pearson's correlation to generate fine vertex-level network assignment maps, based on a winner-takes-all approach similar to an earlier study (Gordon et al., 2017a) (Supplementary Figure 5).

The 23 networks match the fine network divisions in adults and refined our understanding of functional networks in young children.

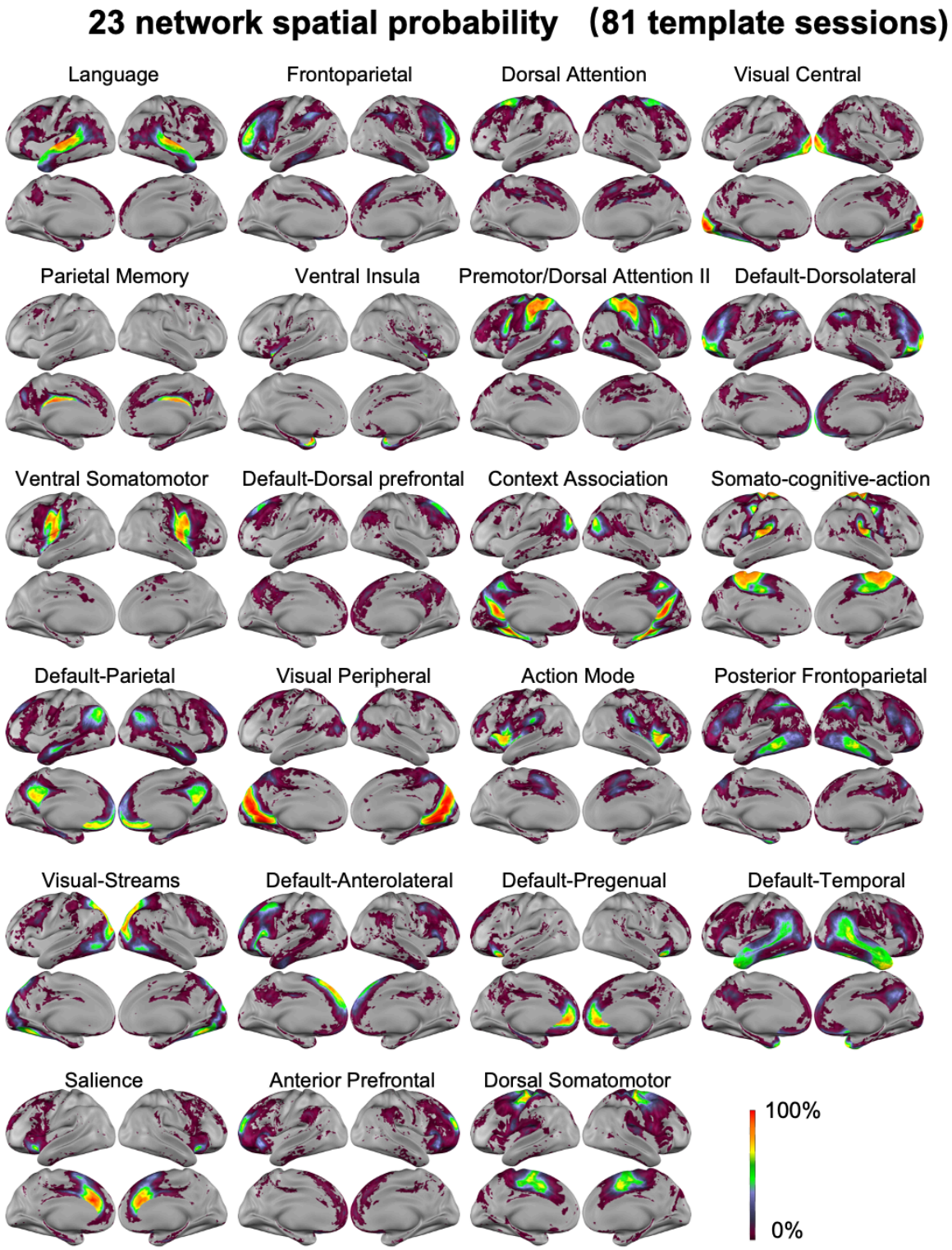

Figure 2. *Functional networks spatial probability.* For each vertex, the spatial probability of the network is quantified as the percentage of sessions within the 81 template sessions with that matching network assignment.

Network spatial probability plots (Dworetsky et al., 2021; Hermosillo et al., 2024; Lipkin et al., 2022; Lynch et al., 2024) show the most and least common locations of a network across the 81 template sessions (Figure 2). To help put the networks into context and relate them to potential behavioral significance, we further applied the Network Correspondence Toolbox (Kong et al., 2025) and "NiMARE: Neuroimaging Meta-Analysis Research Environment" version 0.5.0 (Salo et al., 2023) to compare the topography of our 23 networks to prior literature (Supplementary Figures 6-17, Supplementary Text). Despite the age difference between young children and adults, some of the 23 functional networks have a spatial topography that overlaps with previously identified fine network divisions in adult studies (Du et al., 2024; Gordon et al., 2020; Kong et al., 2019; Lynch et al., 2024). Additionally, the location of less common network occurrences were also consistent with results using highly sampled resting-state fMRI data. For example, we found that the salience network occasionally extends to regions normally assigned to the parietal memory network in some individuals, consistent with a prior report in adults (Kwon et al., 2025). The interdigitation of the Salience (black) and Default-Pregenual (pistachio green) networks at the frontal operculum and the medial prefrontal cortex also resembled the interdigitation of the Salience (black) and Default Mode (red) networks in resting-state fMRI from highly-sampled adult individuals (Braga and Buckner, 2017; Gordon et al., 2017c; Lynch et al., 2024).

To further compare and group the 23 fine network divisions identified here with prior reports in adults, we quantified the similarity between each network to the 20 finely divided adult networks from 45 highly sampled adult individuals (Lynch et al., 2024) based on both network spatial probability maps (Figure 2) as well as the average network FC obtained from averaging FC from all vertices assigned to that network in each subject, and then averaged across subjects (Supplementary Figure 18). Although most of the 23 networks had clear correspondence with the 20 adult networks, some of them (e.g., "Anterior Prefrontal", "Default-Dorsal prefrontal" and "Default-Temporal") did not, potentially suggesting some networks that are present in childhood are later incorporated into other networks in adulthood (Supplementary Figure 19-20). Additionally, there is a much smaller Action Mode Network in young children compared to adults, especially around the dorsal anterior cingulate cortex. Parts of the ventral insula and dorsal somatomotor network in young children might later be incorporated into the Action Mode Network (Supplementary Figure 20). Furthermore, while the frontoparietal network was divided into more cohesive pieces in other studies (Du et al., 2024; Yeo et al., 2011), there was less anterior-posterior bias in the divisions than those reported here.

To aid interpretation and put our networks in the context of existing findings, we made a table summary of previous nomenclature applied to similar network topography in the literature (Table 1), with the caveat that this is only a guideline and some networks may not perfectly overlap with what we described here.

Table 1. Network names and prior mentions

Network number	Network name	Other commonly used names that may overlap with this network and references
1	Language	Language/auditory (Braga et al., 2020; Du et al., 2024; Ji et al., 2019; Lynch et al., 2024), language (Lipkin et al., 2022), auditory language (Zhu et al., 2025), auditory (Kong et al., 2019), ventral attention (Gordon et al., 2016; Power et al., 2011)

2	Frontoparietal	Frontoparietal (Gordon et al., 2017c; Lynch et al., 2024), anterior frontoparietal (Eggebrecht et al., 2017; Kardan et al., 2022), lateral prefrontal (Tu et al., 2025a)
3	Dorsal Attention	Dorsal attention (Lynch et al., 2024), Salience (Braga et al., 2020), CO1/task-control cingulo-opercular subsystem (Gratton et al., 2022), premotor-posterior parietal rostral (Du et al., 2024)
4	Visual Central	Visual central (Du et al., 2024; Yeo et al., 2011)
5	Parietal Memory	Parietal memory (Gordon et al., 2017c; Lynch et al., 2024), Medial parietal (Gordon et al., 2017a)
6	Ventral Insula	Ventral insula (Nomi et al., 2016), orbito-affective (Ji et al., 2019), limbic (Di Plinio and Ebisch, 2018; Yeo et al., 2011), ventral anterior insula (Myoraku et al., 2022)
7	Premotor/Dorsal Attention II	Premotor/Dorsal attention II (Lynch et al., 2024)
8	Default-Dorsolateral	Default-dorsolateral (Gordon et al., 2020; Lynch et al., 2024),
9	Ventral Somatomotor	Ventral somatomotor (Gordon et al., 2017a),Somatomotor face (Gordon et al., 2017c; Lynch et al., 2024), Lateral somatomotor (Laumann et al., 2015)
10	Default - Dorsal prefrontal	Dorsal prefrontal (Alves et al., 2019), prefrontal cortex (Paquola et al., 2025)
11	Context association	Context association (Gordon et al., 2017c), parietal-occipital (Gordon et al., 2017a; Laumann et al., 2015), default-retrosplenial (Lynch et al., 2024)
12	Somato-cognitive-action	Somato-cognitive-action (Gordon et al., 2023; Lynch et al., 2024)
13	Default-Parietal	Default-parietal (Gordon et al., 2020; Lynch et al., 2024), posterior parietal (Alves et al., 2019)
14	Visual Peripheral	Visual peripheral (Du et al., 2024; Yeo et al., 2011)
15	Action Mode	Action mode (Badke D'Andrea et al., 2025; Dosenbach et al., 2025), cingulo-opercular (Gordon et al., 2017a, 2017c; Gratton et al., 2022; Laumann et al., 2015)
16	Posterior fronto-parietal	Posterior frontoparietal (Eggebrecht et al., 2017; Kardan et al., 2022; Tu et al., 2025a)

17	Visual-Streams	Visual-streams (Lynch et al., 2024), visual association (Shen et al., 2013), dorsal attention (Du et al., 2024)
18	Default-Anterolateral	Default-anterolateral (Gordon et al., 2020; Lynch et al., 2024), language (Braga et al., 2020), default semantic (Zhu et al., 2025)
19	Default-Pregenual	Default-pregenual (Gordon et al., 2020), pregenual medial prefrontal cortex (mPFC) (Gordon et al., 2022), pregenual anterior cingulate (pACC) (Palomero-Gallagher et al., 2019)
20	Default-Temporal	Temporal (Kardan et al., 2022)
21	Salience	Salience (Gordon et al., 2017a, 2017c; Laumann et al., 2015; Lynch et al., 2024)
22	Anterior Prefrontal	Anterior prefrontal (Tu et al., 2025a)
23	Dorsal Somatomotor	Dorsal somatomotor (Gordon et al., 2017a), Somatomotor (Laumann et al., 2015), Somatomotor-hand (Gordon et al., 2017c; Lynch et al., 2024)

Individual-specific functional networks in young children are stable within sessions and across longitudinal sessions one year apart.

To examine the individual-specificity of these functional networks, we obtained the individual functional network assignments using the subset of 49 individuals in Dataset 1 with two longitudinal sessions at Y2 and Y3 time points (2.08 ± 0.12 and 3.16 ± 0.24 years old, respectively) with the same procedure described above (Figure 1; Supplementary Figure 5). First, we derived functional networks from the first half and second half of each fMRI session. The consistency of network assignment across the split halves (measured with normalized mutual information, NMI) was significantly higher (two-sample t-test $p<0.001$) within subject (Y2: NMI = 0.4822 ± 0.0669, Y3: NMI = 0.4919 ± 0.0686) than between subjects (Y2: NMI = 0.3274 ± 0.0383, Y3: NMI = 0.3250 ± 0.0379) (Figure 3A, 3C-F), suggesting that the network assignment contain individual-unique features. As a sanity check, the NMI between the network assignments in the first half and the randomly permuted network assignments in the second half is much lower, at approximately 0.001: for Figure 3C, the 95% confidence interval of the permutation null is [0.0013, 0.0016]. To address the potential inflation of NMI by including frames from the same run in the two split halves, we repeated the analysis without overlapping runs and the within-individual NMI was still significantly higher (Supplementary Figure 21, Supplementary Text). To enhance the robustness of our results, we conducted the split-half network reliability analysis in an additional dataset of 8-60 months' children from the Baby Connectome Project (Dataset 2, Supplementary Figure 22). Qualitatively similar results with higher within-subject NMI were obtained (Supplementary Figure 23A-C). Within-subject NMI was positively correlated with the amount (in minutes) of low-motion data in each split-half ($r = 0.6447$, $p < 0.001$), with the total number of minutes of scan time ($r = 0.5781$, $p < 0.001$), and was negatively correlated with the mean framewise displacement of the scan session ($r = -0.1336$, $p = 0.0204$) but was not significantly correlated with age ($r = -0.0553$, $p = 0.3390$;Supplementary Figure 23D). This suggests that the ability to retrieve reliable networks was somewhat limited by the data amount and quality.

To assess longitudinal stability of the individual-specific networks, we also derived individual-specific functional networks from the whole fMRI session for Y2 and Y3 time points of the data collection. Because of the relationship between NMI and amount of data reported above, we decided to use the whole session (Y2: 19.0 ± 4.1 minutes low-motion data, Y3: 18.7 ± 3.7 minutes low-motion data) for this analysis, unlike the prior split-half analysis which used about half of the data amount to generate the networks. The consistency of network assignment across the two longitudinal sessions was significantly higher (two-sample t-test p<0.001) within subject (NMI = 0.5190 ± 0.0444) than between subjects (NMI = 0.3788 ± 0.0330) (Figure 3B, G-H), indicating the individual-specific networks were stable from 2 to 3 years old. While the within-subject NMI value are relatively modest, they are comparable to results from a similar template matching method—albeit using different templates and a different similarity metric—applied to the MSC dataset (a high-quality adult dataset with 5 hours of resting-state fMRI). In that study (Hermosillo et al., 2024), within-subject NMI ranged from 0.527 to 0.648 using all available low-motion data after frame censoring, and was around 0.5 using only 15 minutes of contiguous low-motion data. To further explore the amount of data required to achieve reliability and individual-specificity of the networks, we conducted additional analysis with different lengths of contiguous low-motion data (minimum 2.5 minutes and maximum of 20 minutes in steps of 2.5 minutes; Supplementary Figure 24, Supplementary Text). We found that the within-subject NMI was higher than between-subject NMI with as little as 2.5 minutes of low-motion data $t(2399) = 14.30$, $p < 0.0001$ (Supplementary Table 1), and the two diverged by 7.5 minutes based on confidence interval (Supplementary Figure 24E, Supplementary Text). Taken together, we found that relatively stable individual-specific functional networks can be observed within a scan session and also across longitudinal sessions in children under 5 years old.

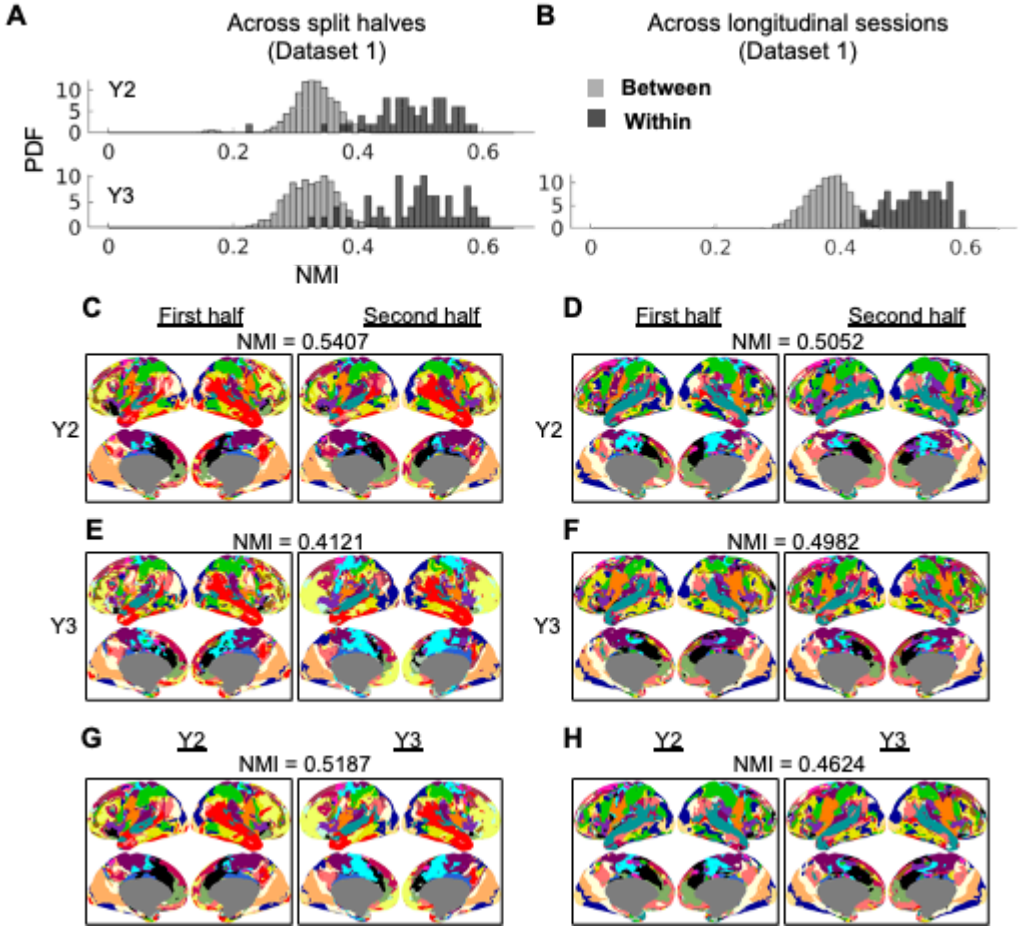

Figure 3. *Individual-specific network topography for 23 networks (Dataset 1, 49 individuals with longitudinal sessions).* A) Within- versus between- individual NMI (across split halves) at Y2 and Y3 time points. PDF: probability density function. B) Within- versus between- individual NMI (across longitudinal sessions). C-D) Network assignments for example individuals at Y2. E-F) Same as C-E but at Y3. G-H) Network assignments for example individuals across the Y2 and Y3 time points.

Population consensus of individual-specific network assignments demonstrated high variability in the lateral frontal cortex, temporal-parietal junction, and the occipital-temporal cortex.

Population consensus (i.e. the most frequent network at each vertex across the population) across all available subjects at Y2 (N = 113, Figure 4A) and at Y3 (N = 86, Figure 4B) of Dataset 1 appears to be similar to each other. Consistent with previous results from adults (Gordon et al., 2017b; Gratton et al., 2018; Kong et al., 2019; Li et al., 2019; Mueller et al., 2013), we found low variability at unimodal processing regions, such as the auditory, visual, and somatosensory and somatomotor cortices, and high variability at the lateral frontal cortex, temporal-parietal junction (TPJ), and the occipital-temporal cortex based on the percentage of subjects with the most frequent assignment (Figure 4C-D). Since this percentage only considered the most frequent assignment but not the frequency of other assignments, we also calculated a complementary "versatility" (Shinn et al., 2017) measure. Vertices that switch assignment among multiple networks across individuals would have a higher versatility than vertices that switch between two networks, even when the most frequent affiliation is the same. The resultant versatility spatial distribution (Supplementary Figure 25) is qualitatively similar to Figure 4C-D. To facilitate comparison to the spatial distribution of the most consistent network assignment reported in older 9 to 10-year-old children (Hermosillo et al., 2024), we also applied a threshold of at least 35%, 45%, 55%, 65% and 75% of individuals on the population consensus network assignments in Dataset 1 (Figure 4E). The locations with the least agreement among participants aligned with the boundaries between network patches, consistent with previous findings in adults where differences in borders among individual participants contributed to the majority of network variability (Dworetsky et al., 2024; Gordon et al., 2017b).

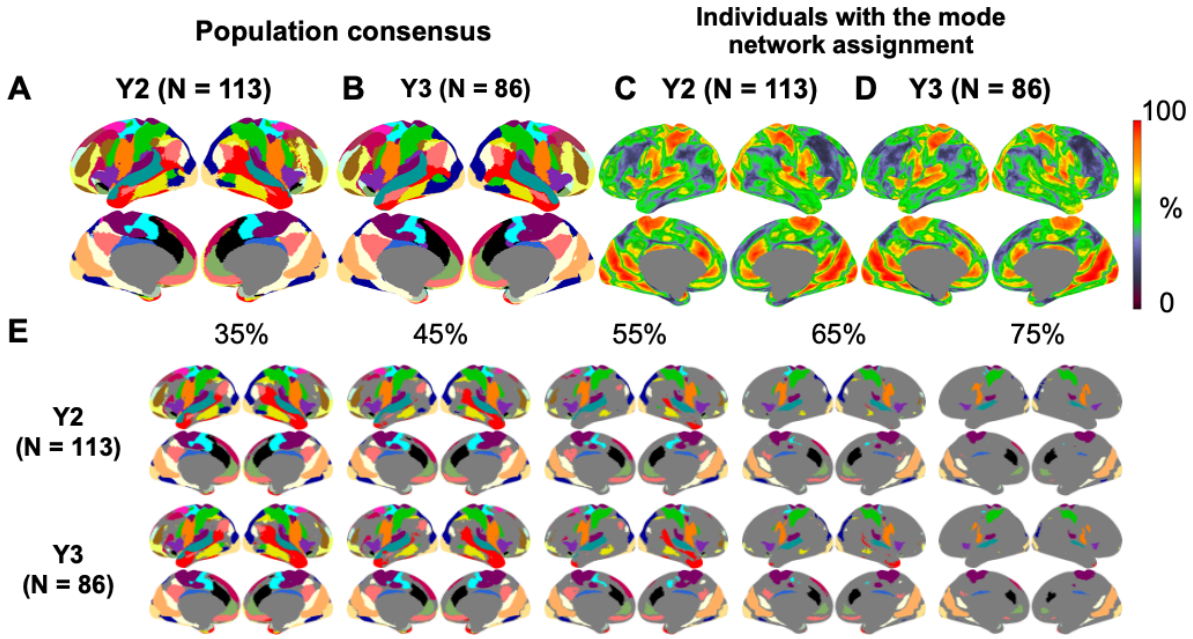

Figure 4. *Population consensus network patterns (most frequent assignment) across subjects (Dataset 1).* A) Population consensus (Y2, 113 subjects). B) Population consensus (Y3, 86 subjects). C-D) Percentage of subjects with the same assignment as the most frequent assignment. E) Population consensus of network identity for only the locations with consistent assignment among at least 35%, 45%, 55%, 65% and 75% subjects.

Developmental variability in hemispheric lateralization is reflected in the individual-specific functional network topography

Given findings from prior literature about network lateralization, especially in the language networks, we sought to test the hypothesis that language-related networks increase in lateralization in young children and that the lateralization relates to the individual child's language ability. We focused on two networks that contain regions commonly reported to be involved in language functions (Braga et al., 2020; Lipkin et al., 2022; Zhu et al., 2025): the language network (Network 1) and the default-anterolateral network (Network 18).

Across children scanned at 8 to 60 months (Dataset 2), the language network primarily includes the superior temporal gyrus (STG), which supports auditory language processing. However, it sometimes incorporates the inferior frontal gyrus (IFG) and middle frontal gyrus (MFG), key components of the adult language network (Braga et al., 2020; Lipkin et al., 2022) that additionally contribute to domain-general processing (Fedorenko and Blank, 2020; Koyama et al., 2017) (Figure 5A, red arrows). Most frequently, the IFG and MFG were assigned to the default-anterolateral network (Figure 5B, red arrows). Compared to participants aged 8–10 months, children at 30–36 months had higher probability of left-hemisphere involvement and lower probability in the right hemisphere involvement for both networks, resulting in increased network lateralization across age (Figure 5C-H).

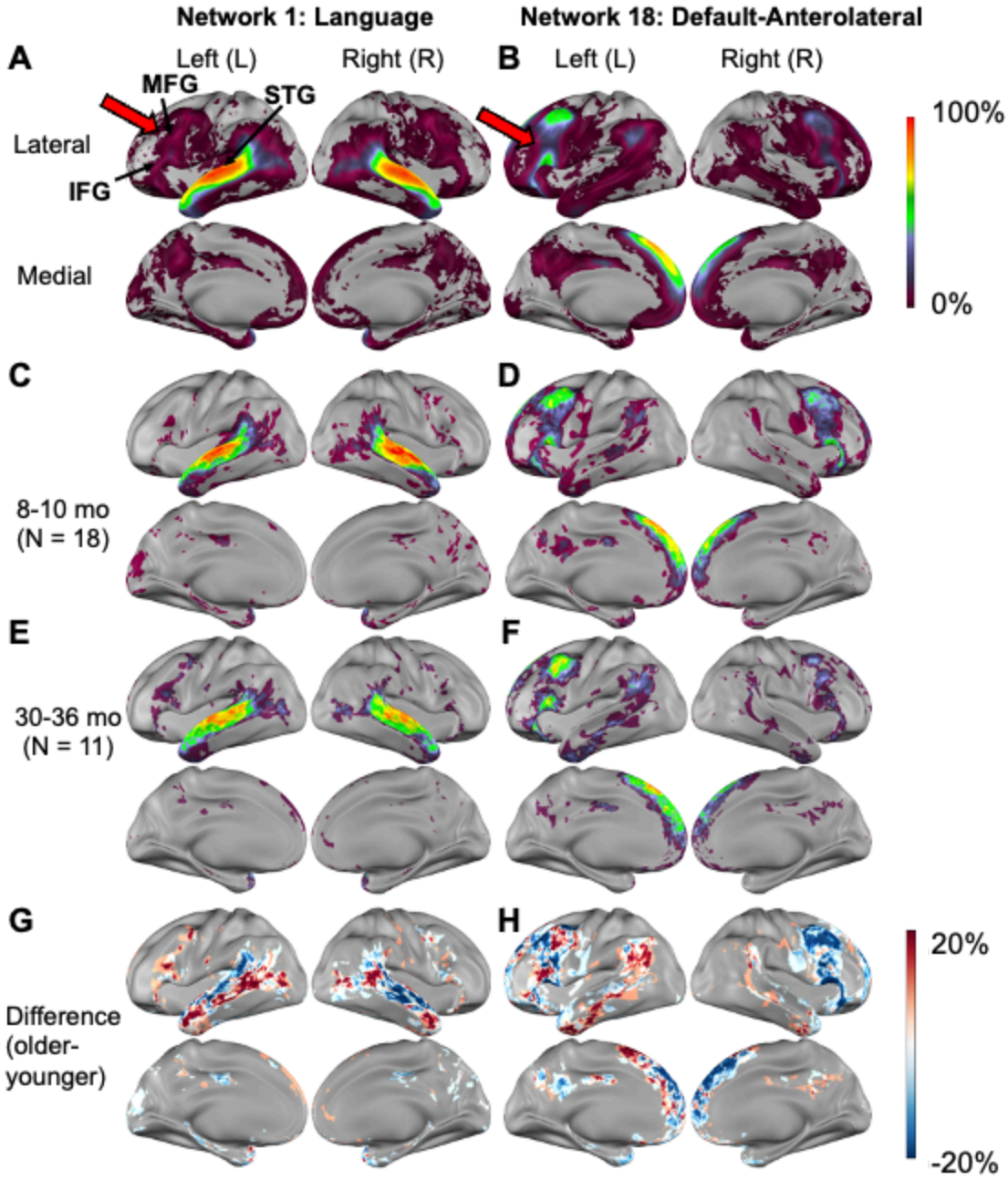

Figure 5. *Spatial probability of Language and Default-Anterolateral networks.* A) Language network probability and B) Default-Anterolateral network probability in children at 8-60 months (Dataset 2). C) Language network probability and D) Default-Anterolateral network probability at 8-10 months. E) Language network probability and F) Default-Anterolateral network probability at 30-36 months. G-H) Difference between the older and younger groups. MFG: Middle Frontal Gyrus, IFG: Inferior Frontal Gyrus, STG: Superior Temporal Gyrus.

To quantify network lateralization, we calculated a "laterality index" (LI) defined as the difference in the network surface areas of a given network between the left and right hemispheres as a percentage of the total network surface area. In children at 8–60 months (Dataset 2), the Language network showed weak left-lateralization (LI = 0.07 ± 0.13, one-sample t-test, $t(300) = 9.2858$, $p < 0.001$), while the Default-Anterolateral network showed

strong left-lateralization (LI = 0.40 ± 0.19, t (300) = 37.1876, $p < 0.001$). LI also positively correlated with age across in both networks, although the effect was not significant for the Language network (r = 0.11, p = 0.0651; Figure 6A) and significant for the Default-Anterolateral network (r = 0.20, $p < 0.001$; Figure 6B). We further tested whether the effect of age on Mullen Verbal Developmental Quotient (VDQ, an age-normalized metric from the Mullen Scales of Early Learning assessment;Mullen, 1995)) was mediated by network laterality, after excluding the 21 subjects without a VDQ score. Using nonparametric bootstrap mediation (5,000 simulations) from the R package "mediation", the average causal mediation effect (ACME) was small and not statistically significant (ACME = 0.43, 95% CI [-0.05, 1.23], p = 0.09 for Language and ACME = 0.50, 95% CI [–0.09, 1.25], p = 0.11 for Default-Anterolateral). The proportions of the total effect mediated by LI (Language) and LI (Default-Anterolateral) were modest (11% and 13%, respectively). Because VDQ is age-normalized, age explains only a small portion of variance in the outcome, which likely limited the indirect effect that network lateralization could mediate. Qualitatively similar results were observed with Dataset 1 (22-47 months), where both the Language network (LI = 0.13 ± 0.16, one-sample t-test, t (198) = 11.2807 , $p < 0.001$) and the Default Anterolateral network (LI = 0.44 ± 0.17, one-sample t-test, t (198) = 37.0012 , $p < 0.001$) were left lateralized. Here, age-normalized Bayley Scales of Infant and Toddler Development language and motor composite scores (Bayley, 2012) were used in place of VDQ and NVDQ for dataset 1 (missing one participant's data at Y2). In this case, age was significantly correlated with the LI of the Language network (r = 0.20, p = 0.0052)(Supplementary Figure 26A) but not the Default-Anterolateral network (r = 0.05, p = 0.4875)(Supplementary Figure 26B). Because the age distribution in Dataset 1 was heavily concentrated around 2 and 3 years, it is possible that the relationship between age and Default-Anterolateral network lateralization was stronger earlier in development, resulting in a weaker effect in this sample.

We also examined whether children's verbal and nonverbal skills were associated with the network lateralization beyond the effect of age. In Dataset 2, we obtained the LI residuals after regressing age with a linear model, and then correlated these LI residuals with VDQ and NVDQ, excluding 21 subjects without VDQ and 19 subjects without NVDQ for the respective analyses. VDQ was significantly correlated with the Language network LI residuals (r = 0.17, p = 0.0040; Figure 6C), but not with the Default-Anterolateral network LI residuals (r = 0.11, p = 0.0764; Figure 6D). NVDQ also showed a marginally significant correlation with the Language network LI residuals (r = 0.13, p = 0.0327, Figure 6E) but not with the Default-Anterolateral network LI residuals (r = 0.08, p = 0.1947; Figure 6F). In Dataset 1, the Bayley language composite scores was significantly correlated with the language network LI residuals (r = 0.15, p = 0.0302; Supplementary Figure 26C), but not with the Default-Anterolateral network (r = 0.11, p = 0.1285; Supplementary Figure 26D), and neither network's LI reisudals were significantly correlated with Bayley motor composite scores (Supplementary Figure 26 E-F).

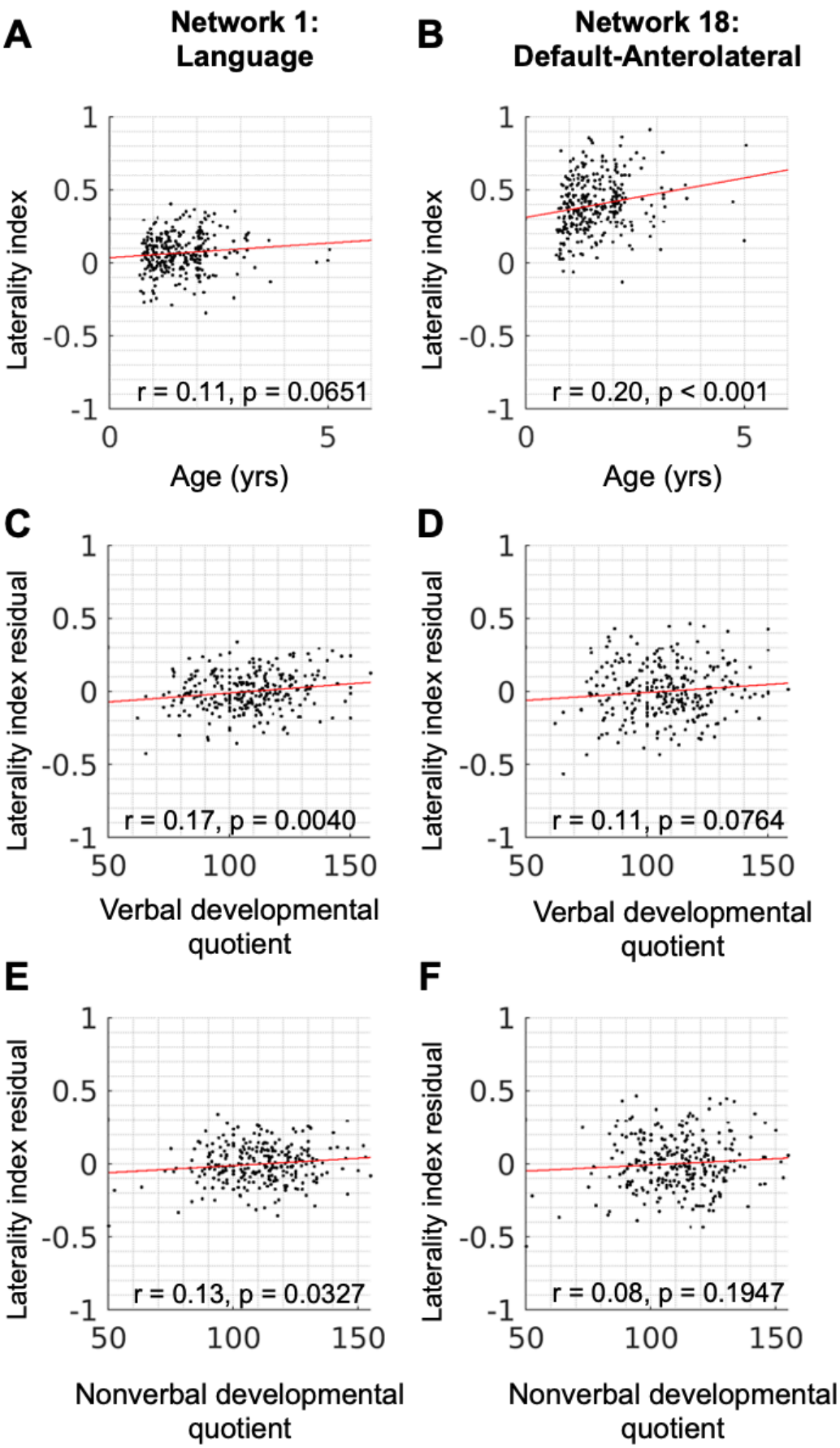
A
Network 1:
Language
B
Network 18:
Default-Anterolateral
Laterality index
Age (yrs)
r = 0.11, p = 0.0651
r = 0.20, p < 0.001
C
D
Laterality index residual
Verbal developmental quotient
r = 0.17, p = 0.0040
r = 0.11, p = 0.0764
E
F
Nonverbal developmental quotient
r = 0.13, p = 0.0327
r = 0.08, p = 0.1947

Figure 6. *The relationship between functional network laterality and age or Mullen Scales of Early Learning developmental quotients.* Laterality index against A-B) age, C-D) verbal developmental quotient, E-F) non-verbal developmental quotient.

Template-matching with the data-driven 23-network templates produces less ambiguous network topography and higher-quality matches

An alternative to a data-driven clustered centroid on FC profiles of all individuals for the network templates (Figure 1) is to use the networks assignments from group-average FC (Tu-19 networks (Tu et al., 2025a), Supplementary Figure 27). As predicted, the quality of separation of the FC profiles was much lower when the network assignments from group-average FC were used (average silhouette index = 0.0337, Supplementary Figure 28A-B), as opposed to the optimized clusters across the population (average silhouette index = 0.1551, Supplementary Figure 28C-D). The distribution of correlation values between the individual FC profiles to their cluster centroids are higher and less skewed in the optimized clusters than the cluster assignments from the Tu-19 networks based on group-average FC (Supplementary Figure 29), indicating that the FC separation is better defined using the 23-network solution.

We repeated the template matching procedure using the group-average prior (Tu-19 networks). For most networks that appear in both the data-driven and group-average priors, their spatial topographies were largely similar. However, the data-driven prior more finely differentiated certain regions. For example, it separates the “Dorsal Somatomotor” found in the group-average prior into two distinct networks: a refined “Dorsal Somatomotor” network, encompassing hand and foot effector regions, and a “Somatic-Cognitive Action” network for integrating goals, physiology and body movement (Gordon et al., 2023). Additionally, when using the group-average prior, we observed broader regions of low template correlation around network boundaries (Supplementary Figure 30). This likely reflects the fact that the group-average templates are spatially blurred and may contain mixed signals from adjacent networks, leading to low-confidence assignments at the edges under the winner-takes-all matching approach.

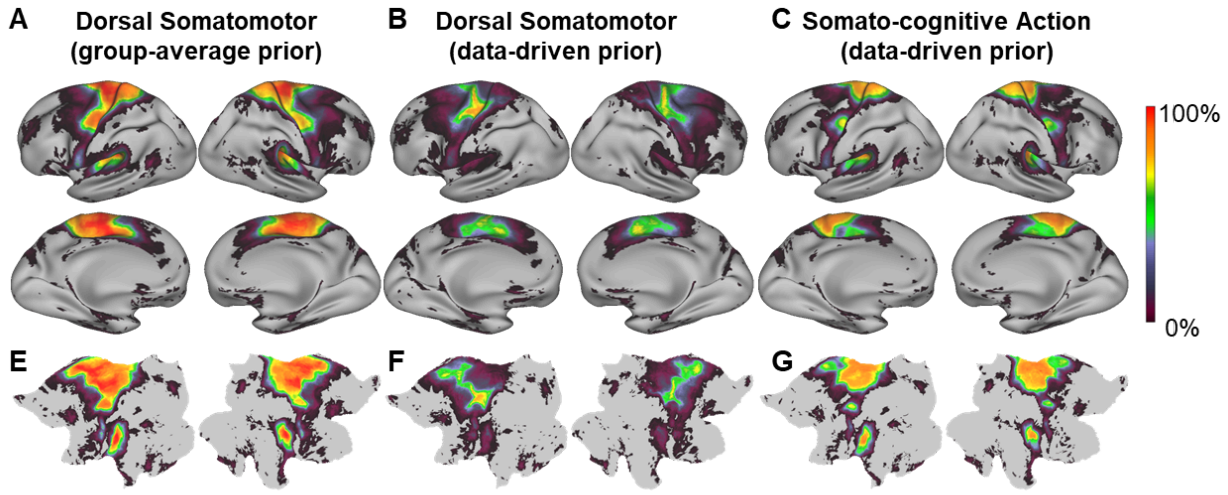

Figure 7. *Network spatial topography of similar networks using group-average prior versus data-driven prior.* A) Dorsal Somatomotor (group-average prior). B) Dorsal Somatomotor (data-driven prior). C) Somato-cognitive Action (data-driven prior). D-F) Same as A-C but viewed in flat maps.

Discussion

A fine network division for developmental detail

Many existing studies have demonstrated residual differences in functional network organization across adult individuals despite anatomical alignment (Bijsterbosch et al., 2023; Braga and Buckner, 2017; Dworetsky et al., 2021; Gordon et al., 2017c, 2017b; Gratton et al., 2018). With young children, there may be even more variability in functional template localization given the substantial amount of developmental changes in the brain during this period (Bethlehem et al., 2022). Smaller and more variable networks risk being obscured by the averaging of anatomically matched locations, and templates created from averaging within a generic network mask will be contaminated by signals from neighboring networks in individual subjects.

By design, individual networks generated from template matching and their population consensus resemble the network priors used in the creation of templates. Although some studies have tried to derive infant-specific network templates (Moore et al., 2024), they were still using a coarse adult network atlas to derive the templates. Moreover, a considerable amount of evidence suggests that there are finer network divisions in individuals than are present in many commonly used adult network atlases (Badke D'Andrea et al., 2025; Braga and Buckner, 2017; Gordon et al., 2023, 2020; Gratton et al., 2022; Lynch et al., 2024). Additional network detail may help capture subtle changes in development.

Here, we created templates directly on concatenated data instead of group-average data. By avoiding averaging FC at matching anatomical locations across individuals, we uncovered functional network patterns that are more representative of the individual FC profiles assigned to that network. These templates also produced better separation of neighboring networks. Our findings improved upon the current standard practice of averaging FC data across individuals even when the goal is to find group-level functional networks. For example, the population consensus division of the anterior temporal lobe reported here is more consistent with previous observations in adults (Akiki and Abdallah, 2019; Andrews-Hanna et al., 2010; Braga and Buckner, 2017; Du et al., 2024; Gordon et al., 2017c, 2016; Ji et al., 2019; Yeo et al., 2011), compared to the divisions identified directly in a group-average FC (Tu et al., 2025a).

Precision functional mapping with a moderate scan length for scalability

Approximately 10 minutes of data can yield a moderate reliability of NMI = 0.46 in individual networks created from longitudinal sessions at 2 and 3 years old, but a longer scan than 10 minutes further increases the reliability of individual-specific networks up to and likely beyond 20 minutes (Supplementary Figure 24). Our results suggest that scan time per individual and data quality persist as a challenge in precision brain mapping (Du et al., 2024; Lynch et al., 2024), echoing claims from one recent study advocating for longer scan times per participant (Ooi et al., 2025). We reason that while high-quality data samples with many hours of fMRI data can be useful for data-driven exploration of individual-specific networks (Gordon et al., 2017c; Kwon et al., 2025; Laumann et al., 2015; Lynch et al., 2024) and within-subject study designs (Huth et al., 2016; Newbold et al., 2020), datasets with more moderate amount of data (e.g. 30 minutes to an hour, following recommendations in Ooi et al., 2025) per participant in relatively large number of participants may be used to increase the quality of group prior-based mapping of individual-specific networks. In line with this idea, recent papers found that a more extensive data collection is required to reach FC reliability in pediatric samples compared to adults, with diminishing returns after 40–50 minutes of post-censoring data (Moser et al., 2025; Rai et al., 2025). Since precise characterization of individual functional networks has been demonstrated to have clinical significance such as improving the efficacy of targeted brain stimulation (Cash et

al., 2021; Lynch et al., 2022; Nahas et al., 2025), fast precision functional mapping with a moderate scan length using a network template offers a scalable solution for unique populations, broadening its potential applications. Further validation is required to assess the utility and data required of prior-based network mapping in those applications.

Individual-specific functional network topography bridges brain specialization with behavioral development

We observed a link between functional network lateralization in the language network and language behavioral performance, beyond the effect of age. In contrast to the strong association between Language network lateralization and the verbal developmental quotient, the association for the Default-Anterolateral network is relatively weaker and statistically insignificant. This finding is consistent with prior studies in school-age children. In particular, greater resting-state laterality in the temporal gyrus but not the inferior frontal gyrus, has been positively correlated with linguistic skills (Day et al., 2024). This observation might be explained by the additional domain-general processing function of the IFG and MFG (Default-Anterolateral network) beyond language processing (Fedorenko and Blank, 2020; Koyama et al., 2017). While these findings alluded to the behavioral significance of the individual-specific functional networks and their potential utility in clinical applications in young children, such as presurgical or brain stimulation site planning, further validation is required to assess the amount of data needed for a reliable application of the individual-specific networks. Additionally, task-based activation is required to confirm the correspondence between the resting-state network topography and the functional co-localization.

Functional network assignments are more consistent at sensory cortices than association cortices.

Consistent with prior results in infants/toddlers (Gao et al., 2014; Molloy and Saygin, 2022; Xu et al., 2019), school-age children (Cui et al., 2020; Hermosillo et al., 2024), and adults (Du et al., 2024; Dworetsky et al., 2021; Gordon et al., 2017b; Gratton et al., 2018; Kong et al., 2019; Langs et al., 2016; Laumann et al., 2015; Li et al., 2019; Miranda-Dominguez et al., 2014; Mueller et al., 2013), we observed higher inter-individual variability of functional network topography in the association cortices than the sensory cortices in young children (Figure 2). As described in prior works (Hill et al., 2010; Tu et al., 2025b), this spatial bias in inter-individual variability may have a developmental origin: early maturation in some areas limits future plasticity. Additionally, the early-developing sensorimotor areas may be more evolutionarily primitive (Hill et al., 2010) and therefore genetically determined to be more consistent across human individuals. One recent paper examining the cell-type abundance in resting-state network divisions in post-mortem brain tissues seemed to support both ideas: the authors observed that sensorimotor network affiliations were better predicted by cell-type than association network affiliations, suggesting more stereotypical cell-type profiles in the sensorimotor networks (Zhang et al., 2024). The contribution of each factor to this observation is awaiting future exploration.

Limitations and future directions

One large difference between extant neuroimaging data in young children and other populations is that most young children were scanned during natural sleep. A large amount of literature illustrates the differences in FC during sleep and those estimated during resting wakefulness (Horovitz et al., 2009; Larson-Prior et al., 2011, 2009; Mitra et al., 2015; Tagliazucchi et al., 2013), and even across different sleep stages (Tagliazucchi et al., 2012; Yang et al., 2024). Babies sleep much longer than adults, with up to 16 hours of sleep per day in neonates and 12 hours in 2-to-3-year-olds. Additionally, the sleep pattern is also different in

neonates under 2 months of age, with up to 50% of sleep time spent in the REM/active sleep stage, compared to around 20% in adults (Roffwarg et al., 1966). Therefore, some of the developmental differences described here are potentially attributable to differences in the sleep-stage composition of fMRI data across different developmental stages.

While our choice of clustering on FC profiles with area parcels as seeds increased the computational efficiency substantially, it may have averaged out some fine spatial detail, limiting the number of functional networks that can be reliably identified across the population. Additionally, more extensive validation with task fMRI (Braga et al., 2020; Du et al., 2024; Nielsen et al., 2023) and more behavioral phenotype prediction (Cui et al., 2020; Kong et al., 2019; Lynch et al., 2024) is required to assess the behavioral significance of our individual-specific functional networks.

Even though we only assigned cortical vertices to functional networks in the current study, the conceptual template matching framework is transferable to subcortical network assignments (Ji et al., 2019; Seitzman et al., 2020). Moreover, functional profiles based on task/movie responses (Haxby et al., 2020; Meschke et al., 2023; Zhi et al., 2022), and potentially even a combination of both response and connectivity (Busch et al., 2021) could be utilized to further increase the reliability of the mapped network.

Materials and Methods

Datasets

We used two high-quality infant/toddler datasets spanning approximately 1-5 years (total number of participants = 341) for the current study. An overview is provided in Table 2, and details of the demographics, acquisition, and processing of the data were reported in other studies with slight differences in the selection of final samples to include (Tooley et al., 2024; Tu et al., 2025a) and are briefly recapitulated below.

Table 2. Dataset summary

Datasets	# Participant	# Sleeping Sessions
Dataset 1: eLABE	150	199
Dataset 2: BCP	178	301

Dataset 1: Early Life Adversity, Biological Embedding (eLABE)

Demographics. We used the Y2 (approximately 2 years old) and Y3 time (approximately 3 years old) point data from the eLABE study with a longitudinal data collection design as our discovery dataset, with basic demographic information summarized in Supplementary Figure 2. This study was approved by the Human Studies Committees at Washington University in St. Louis, and informed consent was obtained from a parent of all participants. Recruitment oversampled mother-infant pairs facing adversity (e.g., poverty and stress). At each time point, all participants with at least 8 minutes of usable low-motion fMRI data and no major quality issue in the structural or functional MRI were included, resulting in a total of 150 participants and 199 sessions, of which 49 individuals had both Y2 and Y3 sessions. A subset of 81 sessions (40 from Y2 and 41 from Y3) from healthy term-born toddlers had more than 20 min of usable low-motion data and were used to generate the network templates.

MRI data acquisition. MRI data were acquired during natural sleep without sedating medications using a 3T Prisma scanner (Siemens Corp.) and 64-channel head coil loosely

following HCP-style acquisition parameters. During each scan session, a T1-weighted image was collected (sagittal, 208 slices, 0.8-mm isotropic resolution, repetition time = 2400 ms, echo time = 2.22 ms). Functional imaging data (fMRI) were collected using a blood oxygen level–dependent (BOLD) gradient-recalled echo-planar multiband sequence (72 slices, 2.0-mm isotropic resolution, echo time = 37 ms, repetition time = 800 ms, multiband factor = 8, 420 volumes) for a total of 2-9 runs (5.6 minutes each). Spin-echo field maps (at least 1 anterior–posterior and 1 posterior-anterior) were obtained during each session with the same parameters. Framewise Integrated Real-time MRI Monitoring (FIRMM) software suite was used to monitor motion summary in realtime (Dosenbach et al., 2017).

MRI data preprocessing. Anatomical scan processing and segmentation were conducted using Freesurfer 7.2. Field distortion correction was performed using the FSL TOPUP toolbox. Functional data preprocessing followed established procedures (Power et al., 2014), which includes the basic correction of intensity differences attributable to interleaved acquisition, bias field correction, intensity normalization of each run to whole-brain mode value of 1000, linear realignment within and across runs to compensate for rigid body motion, and linear registration of BOLD images to the adult Talairach isotropic atlas performed in one single step that includes the BOLD to individual T1 to group-average T1 from this cohort to 711-2N Talairach atlas. Subsequently, volumetric resting-state BOLD time series were projected to fs_LR-32k aligned surfaces for each individual using spherical registration and smoothed with geodesic 2D Gaussian kernels ($\sigma = 2.25$ mm) (Van Essen et al., 2012). Additional fMRI preprocessing to mitigate the effect of motion and other non-neuronal sources of signal was conducted with (i) demean and detrend, (ii) nuisance regression including white matter, ventricles, extra-axial cerebrospinal fluid, and the whole brain mean signals and the 24-parameter Friston expansion regressors derived from the 6 rigid body realignment parameters (x, y, z, pitch, yaw, roll), (iii) bandpass filtering to 0.005-0.1 Hz (Power et al., 2014) after the BOLD data was mapped to surface. Framewise displacement (FD) was calculated to index the amount of motion within each session and for the creation of a motion censoring time mask. Specifically, the 6 rigid body realignment parameters were first filtered with an age-specific respiratory notch filter (0.27-0.5 Hz) to reduce the impact of artifactual motion introduced by B0 field perturbation (Fair, 2020; Kaplan et al., 2022). FD was then calculated as the sum of the absolute values (L1-norm) of the differentiated notch-filtered 6 rigid body realignment parameters (by backwards differences) at every time point, with the FD of the first frame set to 0 by convention. fMRI data were then censored based on a threshold of $FD_{filt} > 0.2$ mm, with the additional restriction that only epochs of at least 3 consecutive frames $FD_{filt} < 0.2$ mm were included, and the first X frames were also excluded. Lastly, due to imperfect registration of the medial wall, a small subset of vertices were missing data at the hippocampal regions, and were imputed by the mean value of the nearest neighbor using a custom MATLAB script.

Dataset 2: Baby Connectome Project (BCP)

Demographics. Full-term (gestational age of 37-42 weeks) infants free of any major pregnancy and delivery complications were recruited as part of the Baby Connectome Project (Howell et al., 2019). All procedures were approved by the University of North Carolina at Chapel Hill and the University of Minnesota Institutional Review Boards. Informed consent was obtained from the parents of all participants. In the final cohort used following fMRI data quality control, we retained 301 sleeping fMRI sessions from 178 individuals acquired during natural sleep.

MRI data acquisition. All MRI images were acquired on a Siemens 3T Prisma scanner with a 32-channel head coil at the University of Minnesota and the University of North Carolina at Chapel Hill during natural sleep without the use of sedating medications. T1-weighted

(TR=2400 ms, TE=2.24 ms, 0.8 mm isotropic; flip angle = 8°), T2-weighted images (TR=3200 ms, TE=564 ms, 0.8 mm isotropic), spin echo field maps (SEFM) (TR=8000 ms, TE=66 ms, 2 mm isotropic, MB=1), and fMRI data (TR=800 ms, TE=37 ms, 2 mm isotropic, MB=8) were collected. A mixture of Anterior→Posterior (AP) and Posterior→Anterior (PA) phase encoding directions was used for fMRI acquisition in each session, but they were concatenated into one time series. A subset of data (88 sleeping sessions) had a 720-ms TR instead of an 800-ms TR.

MRI data preprocessing. Data processing used the DCAN-Labs infant-abcd-bids-pipeline (v0.0.22), which largely follows the HCP processing (Glasser et al., 2013) and the steps described previously for the ABCD dataset (Feczko et al., 2021). The processing steps were similar to the adult data except for the use of infant-specific MNI templates to better register the structural data. In addition, segmentation of the brain structures was conducted with Joint Label Fusion (JLF). The toddler-specific brain mask and segmentation were substituted for the Freesurfer (Fischl, 2012) pipeline to refine the white matter segmentation and guide the FreeSurfer surface delineation for each individual scan session of each participant. The native surface data were then deformed to the fs_LR-32k template via a spherical registration.

Functional data processing was largely the same as before, except for the following minor differences: (i) across-run intensity normalization to a whole-brain mode value of 10,000 instead of 1000. (ii) An infant MNI template was used for registration. (iii) fMRI BOLD volumes were sampled to native surfaces using a ribbon-constrained sampling procedure available in Connectome Workbench and then deformed and resampled from the individual's “native” surface to the fs_LR-32k surface with minimal smoothing at $\sigma = 0.85$ mm. Additional steps to mitigate the non-neuronal sources of artifact was conducted on the surface data similar to Dataset 1 with a few minor differences: (i) the mean signal of extra-axial cerebrospinal fluid was not included in the regression, and the mean signals of the 91k grayordinates substituted the whole-brain signal in the nuisance regression, the first-order derivative of the white matter, ventricular CSF and been grayordinate signals were also included for nuisance regression (ii) a respiratory notch filter (0.28-0.48 Hz) (Fair, 2020; Kaplan et al., 2022) was applied to the motion parameters estimates before both FD calculation and the construction of the 24-parameter Friston expansion regressor. (iii) fMRI data were then censored based on a threshold of $FD_{filt} > 0.2$ mm, and the first 7 frames were also excluded. Subsequently, outlier frames whose across-grayordinate standard deviation was more than 3 median absolute deviations from the median of all frames included, and individual runs were further excluded from a very small subset of sessions due to failure of the visual quality check. A further smoothing with a geodesic 2D Gaussian kernel ($\sigma = 2.40$ mm) was applied to give a final effective smoothing of $\sigma = 2.55$ mm. We then focused on only the 59412 cortical vertices (excluding medial masks) in the fs_LR-32k surface for the subsequent analyses.

Creation of functional connectome

Three types of functional connectome were used. The vertex-to-vertex functional connectome was used to assign network labels to individual vertices based on the atlas-driven network templates (vertex-resolution), and the parcel-to-parcel functional connectome was used to build the data-driven network templates (parcel-resolution). And lastly, the vertex-to-parcel functional connectome was used to assign network labels to individual vertices based on the data-driven network templates (parcel resolution). In each case, the BOLD time series of each vertex or each parcel (calculated by averaging across all vertices in the parcel) from the Tu-326 parcel atlas previously demonstrated to fit this age range (Tu et al., 2025a) was correlated with the BOLD time series of each vertex or each parcel across the whole neocortex in the left and right hemisphere.

Data-driven template creation

Additionally, we also directly identified a set of network templates using a data-driven procedure independent of an atlas. Specifically, we concatenated the parcel-by-parcel (326×326) functional connectomes from 81 template sessions (from 72 unique participants) to a single matrix with 26406 (326×81) samples and 326 dimensions (Figure 4A). A K-means clustering with K = 23, correlation distance as the distance measure, and initial centroid position determined by the k-means++ algorithm (default) was conducted in MATLAB (rationale for hyperparameter choices mentioned in the section below). Because the K-means solution is susceptible to the initial centroid location, we set the number of times to repeat the clustering to 1000 to minimize the possibility of stopping at a local minimum. The output of K-means is the cluster assignment (1 to 23) for each of the 26406 samples (a.k.a. one parcel in one session) and K cluster centroids, which were subsequently used as network templates for template matching.

K-means hyperparameter choices

To find the optimal parameter for K, we use a stability analysis. The intuition is that different subsamples of the data would result in similar cluster centroids if the number of clusters matches the true data structure (Lange et al., 2004; Yeo et al., 2011). Specifically, the 81 sessions were split into halves (41 and 40 sessions) randomly 20 times and made two concatenated matrices similar to the section above. For each time, a K-means clustering with K = 1 to 40, correlation distance as the distance measure, and initial centroid position determined by the K-means++ algorithm was conducted in MATLAB on each of the split-half sessions separately. The maximum number of 40 clusters was motivated by the number of functional networks most commonly reported in neuroimaging research (Power et al., 2011; Yeo et al., 2011). Next, the two sets of centroids from K-means output were used to predict the cluster membership of the second split-half data by assigning it to the nearest centroid. The stability is then measured as the normalized mutual information (NMI) between the cluster memberships predicted by the first set of centroids and the second set of centroids. Because our goal is not to find the best centroid but rather to identify the appropriate number of K, the replication of K-means random initiations was set to 100 instead of 1000 to lower the computational load. As a result, we get 20 NMI measures for each K (Figure 3B). The best K (K = 23) was identified as the largest K before stability starts to drop (local peak).

Obtain individual-specific functional networks through template matching

Seed-based FC analysis using voxels/vertices or ROIs as seed nodes to measure its functional connectivity to the whole cortex/whole-brain is a popular technique to define resting-state networks (Biswal et al., 1995; Fox et al., 2005; Greicius et al., 2003). We identified the network template with the smallest correlation distance, defined as 1-Pearson's correlation, to the seed FC (MATLAB script: pdist2(seed FC, template-FC, 'corr', 'Smallest', 1)). Importantly, the seed FC and template FC can be calculated with respect to all cortical vertices, or a subset of vertices/parcels as targets, similar to the section above. Unlike prior implementations (Dworetsky et al., 2021; Gordon et al., 2017a; Hermosillo et al., 2024; Moore et al., 2024), we did not impose a magnitude threshold to keep only the strongest functional connectivity or a distance threshold to remove the most proximal functional connectivity, because we want to reduce the number of arbitrary decisions for data manipulation, and our experience with using the Dice score to calculate the similarity of binarized FC profiles significantly extended the computational time and sometimes results in ambiguous matches with the same score. Additionally, weaker or even anticorrelations may still have a role in distinguishing functional networks (Chang and Glover, 2009; Dosenbach et al., 2025; Fox et al., 2005; Rubinov and

Sporns, 2011; Uddin et al., 2009), and demonstrated the largest difference between adults and neonates (Sylvester et al., 2022), so we chose to retain all connections.

Reliability of individual-specific functional networks

One way to measure reliability is to compare the individual-specific functional networks generated using different data samples from the same session. We split the number of low-motion frames into the first half and second half of the session and calculated two functional connectomes. Then, we generated the individual-specific functional networks from the two functional connectomes and compared them using the normalized mutual information (NMI). Similarly, we generated the individual-specific functional networks from the two functional connectomes generated using the fMRI data in Y2 and Y3 time points for the same individual to examine longitudinal reliability.

Nodal versatility

Nodal versatility (V) (Shinn et al., 2017) measures whether a node is consistently assigned (V ≈ 0) to a specific community, or it is inconsistently assigned to different communities (V >> 0) across different partitions (in our case, different individual networks).

Lateralization of individual-specific functional networks

The fsLR-32k surface template does not sample the gyral and sulcal surfaces equally (Feilong et al., 2024). To get an accurate measure of the individual-specific functional network size, we calculated the surface area of each vertex using the Connectome Workbench (version 1.2.3) command “wb_command -surface-vertex-areas” using the participant’s midthickness surface obtained from the structural data in the same scan session. The sizes of a given network in each of the left and right hemispheres were calculated as the sum of the surface area of all vertices assigned to that network in the individual in the corresponding hemisphere. A lateralization index was then calculated as the difference in network sizes in the left hemisphere and right hemisphere, divided by the total network size.

Behavioral measures: Mullen Scales of Early Learning (MSEL)

Mullen Scales of Early Learning (Mullen, 1995) was a standardized assessment of language, motor, and perceptual abilities for children through 5 years of age. There are 5 subdomains: 1) gross motor (GM), 2) fine motor (FM), 3) visual reception (VR), 4) receptive language (RL), and 5) expressive language (EL). The assessment takes 20-45 minutes and was implemented at every behavioral visit between 3 and 60 months of age (Howell et al., 2019). We calculated verbal and non-verbal developmental quotient scores (VDQ and NVDQ) as defined by the formula below with the age-equivalent (AE) scores from the subdomains (Stephens et al., 2018):

$$VDQ = (receptive\ language\ AE\ score + expressive\ language\ AE\ score)/2)/age_{months} * 100$$

(Equation 1)

$$NVDQ = (visual\ reception\ AE\ score + fine\ motor\ AE\ score)/2)/age_{months} * 100$$ (Equation 2)

Calculating similarity between networks with spatial probability and FC

To put our 23 functional networks in the context of prior literature and determine the hierarchy in the functional networks, we adapted a method from a prior paper to calculate a similarity measure using both the spatial overlap and FC (Lynch et al., 2024). Specifically, the overall similarity is calculated as the product of FC similarity and spatial overlap. In the original code base, binarized infomap community topography was used so the spatial overlap was calculated as the average spatial probability covered by that community. In our study, our network

topography was specified as continuous (probability, ranging from 0 to 1) rather than binarized value, so the spatial overlap of each of our 23 networks and the Lynch network priors was modified to be calculated as the summed product of the spatial probability of that network and the Lynch network priors, divided by the sum of the spatial probability of that network, similar to the conditional probability formula. The final script "pfm_identify_networks_precalculated.m" is available at https://github.com/cindyhfls/PFM, adapted from https://github.com/cjl2007/PFM-Depression.

Quality of separation of the FC profiles

To measure the quality of separations into clusters defined by the network assignments from the group-average FC and the K-means optimized assignments, we use the silhouette index (SI) metric (Rousseeuw, 1987) for each individual FC profile defined as:

$SI = \frac{b-a}{max(a,b)}$ (Equation 1),

where a is the mean correlation distance (i.e. 1-correlation) to all other FC profiles within the assigned cluster, and b is the mean correlation distance to all FC profiles within the best alternative cluster. The SI ranges from +1 to -1 with the sign indicating whether the area has a more similar FC profile within the assigned cluster (+) or to FC profiles in an alternative cluster (-). The magnitude indicates the degree of separation between the clusters.

Acknowledgment

We thank Dr. Julia Moser for their helpful discussions on the template matching procedures, and Dr. Matthew Glasser for suggestions on network nomenclature and Dr. Samuel R. Krimmel for providing the surface-to-volume transformation script. The current study is funded by the NIH (R00EB029343 and R01HD115540 to MDW; R01MH122389, R01MH134966, and R01MH131584 to CMS). The Early Life Adversity, Biological Embedding (eLABE) study was supported by NIMH R01 MH113883. The Baby Connectome Project was supported by NIMH R01 MH104324 and NIMH U01 MH110274.

Reference

Akiki, T.J., Abdallah, C.G., 2019. Determining the Hierarchical Architecture of the Human Brain Using Subject-Level Clustering of Functional Networks. Sci Rep 9, 19290. https://doi.org/10.1038/s41598-019-55738-y

Alves, P.N., Foulon, C., Karolis, V., Bzdok, D., Margulies, D.S., Volle, E., Thiebaut de Schotten, M., 2019. An improved neuroanatomical model of the default-mode network reconciles previous neuroimaging and neuropathological findings. Commun Biol 2, 370. https://doi.org/10.1038/s42003-019-0611-3

Andrews-Hanna, J.R., Reidler, J.S., Sepulcre, J., Poulin, R., Buckner, R.L., 2010. Functional-Anatomic Fractionation of the Brain's Default Network. Neuron 65. https://doi.org/10.1016/j.neuron.2010.02.005

Badke D'Andrea, C., Laumann, T.O., Newbold, D.J., Lynch, C.J., Hadji, M., Nelson, S.M., Nielsen, A.N., Chauvin, R.J., Krimmel, S.R., Snyder, A.Z., Marek, S., Greene, D.J., Raichle, M.E., Dosenbach, N.U.F., Gordon, E.M., 2025. Action-mode subnetworks for decision-making, action control, and feedback. Proceedings of the National Academy of Sciences 122, e2502021122. https://doi.org/10.1073/pnas.2502021122

Bayley, N., 2012. Bayley Scales of Infant and Toddler Development, Third Edition. PsycTESTS Dataset. https://doi.org/10.1037/t14978-000

Bernard, F., Lemee, J.-M., Mazerand, E., Leiber, L.-M., Menei, P., Ter Minassian, A., 2020. The ventral attention network: the mirror of the language network in the right brain hemisphere. Journal of Anatomy 237, 632–642. https://doi.org/10.1111/joa.13223

Bethlehem, R. a. I., Seidlitz, J., White, S.R., Vogel, J.W., Anderson, K.M., Adamson, C., Adler, S., Alexopoulos, G.S., Anagnostou, E., Areces-Gonzalez, A., Astle, D.E., Auyeung, B., Ayub, M., Bae, J., Ball, G., Baron-Cohen, S., Beare, R., Bedford, S.A., Benegal, V., Beyer, F., Blangero, J., Blesa Cábez, M., Boardman, J.P., Borzage, M., Bosch-Bayard, J.F., Bourke, N., Calhoun, V.D., Chakravarty, M.M., Chen, C., Chertavian, C., Chetelat, G., Chong, Y.S., Cole, J.H., Corvin, A., Costantino, M., Courchesne, E., Crivello, F., Cropley, V.L., Crosbie, J., Crossley, N., Delarue, M., Delorme, R., Desrivieres, S., Devenyi, G.A., Di Biase, M.A., Dolan, R., Donald, K.A., Donohoe, G., Dunlop, K., Edwards, A.D., Elison, J.T., Ellis, C.T., Elman, J.A., Eyler, L., Fair, D.A., Feczko, E., Fletcher, P.C., Fonagy, P., Franz, C.E., Galan-Garcia, L., Gholipour, A., Giedd, J., Gilmore, J.H., Glahn, D.C., Goodyer, I.M., Grant, P.E., Groenewold, N.A., Gunning, F.M., Gur, R.E., Gur, R.C., Hammill, C.F., Hansson, O., Hedden, T., Heinz, A., Henson, R.N., Heuer, K., Hoare, J., Holla, B., Holmes, A.J., Holt, R., Huang, H., Im, K., Ipser, J., Jack, C.R., Jackowski, A.P., Jia, T., Johnson, K.A., Jones, P.B., Jones, D.T., Kahn, R.S., Karlsson, H., Karlsson, L., Kawashima, R., Kelley, E.A., Kern, S., Kim, K.W., Kitzbichler, M.G., Kremen, W.S., Lalonde, F., Landeau, B., Lee, S., Lerch, J., Lewis, J.D., Li, J., Liao, W., Liston, C., Lombardo, M.V., Lv, J., Lynch, C., Mallard, T.T., Marcelis, M., Markello, R.D., Mathias, S.R., Mazoyer, B., McGuire, P., Meaney, M.J., Mechelli, A., Medic, N., Misic, B., Morgan, S.E., Mothersill, D., Nigg, J., Ong, M.Q.W., Ortinau, C., Ossenkoppele, R., Ouyang, M., Palaniyappan, L., Paly, L., Pan, P.M., Pantelis, C., Park, M.M., Paus, T., Pausova, Z., Paz-Linares, D., Pichet Binette, A., Pierce, K., Qian, X., Qiu, J., Qiu, A., Raznahan, A., Rittman, T., Rodrigue, A., Rollins, C.K., Romero-Garcia, R., Ronan, L., Rosenberg, M.D., Rowitch, D.H., Salum, G.A., Satterthwaite, T.D., Schaare, H.L., Schachar, R.J., Schultz, A.P., Schumann, G., Schöll, M., Sharp, D., Shinohara, R.T., Skoog, I., Smyser, C.D., Sperling, R.A., Stein, D.J., Stolicyn, A., Suckling, J., Sullivan, G., Taki, Y., Thyreau, B., Toro, R., Traut, N., Tsvetanov, K.A., Turk-Browne, N.B., Tuulari, J.J., Tzourio, C., Vachon-Presseau, É., Valdes-Sosa, M.J., Valdes-Sosa, P.A., Valk, S.L., van Amelsvoort, T., Vandekar, S.N., Vasung, L., Victoria, L.W., Villeneuve, S., Villringer, A., Vértes, P.E., Wagstyl, K., Wang, Y.S., Warfield, S.K., Warrier, V., Westman, E., Westwater, M.L., Whalley, H.C., Witte, A.V., Yang, N., Yeo, B., Yun, H., Zalesky, A., Zar, H.J., Zettergren, A., Zhou, J.H., Ziauddeen, H., Zugman, A., Zuo, X.N., Bullmore, E.T., Alexander-Bloch, A.F., 2022. Brain charts for the human lifespan. Nature 604, 525–533. https://doi.org/10.1038/s41586-022-04554-y

Bijsterbosch, J.D., Farahibozorg, S.-R., Glasser, M.F., Van Essen, D., Snyder, L.H., Woolrich, M.W., Smith, S.M., 2023. Evaluating functional brain organization in individuals and identifying contributions to network overlap. Imaging Neuroscience 1, 1–19. https://doi.org/10.1162/imag_a_00046

Biswal, B., Zerrin Yetkin, F., Haughton, V.M., Hyde, J.S., 1995. Functional connectivity in the motor cortex of resting human brain using echo-planar mri. Magnetic Resonance in Medicine 34, 537–541. https://doi.org/10.1002/mrm.1910340409

Braga, R.M., Buckner, R.L., 2017. Parallel Interdigitated Distributed Networks within the Individual Estimated by Intrinsic Functional Connectivity. Neuron 95, 457-471.e5. https://doi.org/10.1016/j.neuron.2017.06.038

Braga, R.M., DiNicola, L.M., Becker, H.C., Buckner, R.L., 2020. Situating the left-lateralized language network in the broader organization of multiple specialized large-scale distributed networks. Journal of Neurophysiology 124, 1415–1448. https://doi.org/10.1152/jn.00753.2019

Busch, E.L., Slipski, L., Feilong, M., Guntupalli, J.S., Castello, M.V. di O., Huckins, J.F., Nastase, S.A., Gobbini, M.I., Wager, T.D., Haxby, J.V., 2021. Hybrid hyperalignment: A single high-dimensional model of shared information embedded in cortical patterns of response and functional connectivity. NeuroImage 233, 117975. https://doi.org/10.1016/j.neuroimage.2021.117975

Cash, R.F.H., Weigand, A., Zalesky, A., Siddiqi, S.H., Downar, J., Fitzgerald, P.B., Fox, M.D., 2021. Using Brain Imaging to Improve Spatial Targeting of Transcranial Magnetic Stimulation for Depression. Biological Psychiatry, Neurostimulation for Psychiatric Disorders 90, 689–700. https://doi.org/10.1016/j.biopsych.2020.05.033

Chang, C., Glover, G.H., 2009. Effects of model-based physiological noise correction on default mode network anti-correlations and correlations. NeuroImage 47, 1448–1459. https://doi.org/10.1016/j.neuroimage.2009.05.012

Cui, Z., Li, H., Xia, C.H., Larsen, B., Adebimpe, A., Baum, G.L., Cieslak, M., Gur, R.E., Gur, R.C., Moore, T.M., Oathes, D.J., Alexander-Bloch, A.F., Raznahan, A., Roalf, D.R., Shinohara, R.T., Wolf, D.H., Davatzikos, C., Bassett, D.S., Fair, D.A., Fan, Y., Satterthwaite, T.D., 2020. Individual Variation in Functional Topography of Association Networks in Youth. Neuron 106, 340-353.e8. https://doi.org/10.1016/j.neuron.2020.01.029

Damoiseaux, J.S., Rombouts, S. a. R.B., Barkhof, F., Scheltens, P., Stam, C.J., Smith, S.M., Beckmann, C.F., 2006. Consistent resting-state networks across healthy subjects. PNAS 103, 13848–13853. https://doi.org/10.1073/pnas.0601417103

Day, T.K.M., Hermosillo, R., Conan, G., Randolph, A., Perrone, A., Earl, E., Byington, N., Hendrickson, T.J., Elison, J.T., Fair, D.A., Feczko, E., 2024. Multi-level fMRI analysis applied to hemispheric specialization in the language network, functional areas, and their behavioral correlations in the ABCD sample. Developmental Cognitive Neuroscience 66, 101355. https://doi.org/10.1016/j.dcn.2024.101355

Derman, D., Pham, D.D., Mejia, A.F., Ferradal, S.L., 2025. Individual patterns of functional connectivity in neonates as revealed by surface-based Bayesian modeling. Imaging Neuroscience 3, imag_a_00504. https://doi.org/10.1162/imag_a_00504

Di Plinio, S., Ebisch, S.J.H., 2018. Brain network profiling defines functionally specialized cortical networks. Human Brain Mapping 39, 4689–4706. https://doi.org/10.1002/hbm.24315

Dosenbach, N.U.F., Koller, J.M., Earl, E.A., Miranda-Dominguez, O., Klein, R.L., Van, A.N., Snyder, A.Z., Nagel, B.J., Nigg, J.T., Nguyen, A.L., Wesevich, V., Greene, D.J., Fair, D.A., 2017. Real-time motion analytics during brain MRI improve data quality and reduce costs. Neuroimage 161, 80–93. https://doi.org/10.1016/j.neuroimage.2017.08.025

Dosenbach, N.U.F., Raichle, M.E., Gordon, E.M., 2025. The brain's action-mode network. Nat. Rev. Neurosci. 1–11. https://doi.org/10.1038/s41583-024-00895-x

Du, J., DiNicola, L.M., Angeli, P.A., Saadon-Grosman, N., Sun, W., Kaiser, S., Ladopoulou, J., Xue, A., Yeo, B.T.T., Eldaief, M.C., Buckner, R.L., 2024. Organization of the human cerebral cortex estimated within individuals: networks, global topography, and function. Journal of Neurophysiology 131, 1014–1082. https://doi.org/10.1152/jn.00308.2023

Dworetsky, A., Seitzman, B.A., Adeyemo, B., Neta, M., Coalson, R.S., Petersen, S.E., Gratton, C., 2021. Probabilistic mapping of human functional brain networks identifies regions of high group consensus. NeuroImage 237, 118164. https://doi.org/10.1016/j.neuroimage.2021.118164

Dworetsky, A., Seitzman, B.A., Adeyemo, B., Nielsen, A.N., Hatoum, A.S., Smith, D.M., Nichols, T.E., Neta, M., Petersen, S.E., Gratton, C., 2024. Two common and distinct forms of variation in human functional brain networks. Nat Neurosci 27, 1187–1198. https://doi.org/10.1038/s41593-024-01618-2

Eggebrecht, A.T., Elison, J.T., Feczko, E., Todorov, A., Wolff, J.J., Kandala, S., Adams, C.M., Snyder, A.Z., Lewis, J.D., Estes, A.M., Zwaigenbaum, L., Botteron, K.N., McKinstry, R.C., Constantino, J.N., Evans, A., Hazlett, H.C., Dager, S., Paterson, S.J., Schultz, R.T., Styner, M.A., Gerig, G., Das, S., Kostopoulos, P., The IBIS Network, Schlaggar, B.L., Petersen, S.E., Piven, J., Pruett, J.R., Jr, 2017. Joint Attention and Brain Functional Connectivity in Infants and Toddlers. Cerebral Cortex 27, 1709–1720. https://doi.org/10.1093/cercor/bhw403

Fair, D.A., 2020. Correction of respiratory artifacts in MRI head motion estimates. NeuroImage 17.

Feczko, E., Conan, G., Marek, S., Tervo-Clemmens, B., Cordova, M., Doyle, O., Earl, E., Perrone, A., Sturgeon, D., Klein, R., Harman, G., Kilamovich, D., Hermosillo, R., Miranda-Dominguez, O., Adebimpe, A., Bertolero, M., Cieslak, M., Covitz, S., Hendrickson, T., Juliano, A.C., Snider, K., Moore, L.A., Uriartel, J., Graham, A.M., Calabro, F., Rosenberg, M.D., Rapuano, K.M., Casey, B.J., Watts, R., Hagler, D., Thompson, W.K., Nichols, T.E., Hoffman, E., Luna, B., Garavan, H., Satterthwaite, T.D., Ewing, S.F., Nagel, B., Dosenbach, N.U.F., Fair, D.A., 2021. Adolescent Brain Cognitive Development (ABCD) Community MRI Collection and Utilities. https://doi.org/10.1101/2021.07.09.451638

Fedorenko, E., Blank, I.A., 2020. Broca's Area Is Not a Natural Kind. Trends in Cognitive Sciences 24, 270–284. https://doi.org/10.1016/j.tics.2020.01.001

Feilong, M., Jiahui, G., Gobbini, M.I., Haxby, J.V., 2024. A cortical surface template for human neuroscience. Nat Methods 1–7. https://doi.org/10.1038/s41592-024-02346-y

Fischl, B., 2012. FreeSurfer. NeuroImage, 20 YEARS OF fMRI 62, 774–781. https://doi.org/10.1016/j.neuroimage.2012.01.021

Fox, M.D., Snyder, A.Z., Vincent, J.L., Corbetta, M., Van Essen, D.C., Raichle, M.E., 2005. The human brain is intrinsically organized into dynamic, anticorrelated functional networks. Proc. Natl. Acad. Sci. U.S.A. 102, 9673–9678. https://doi.org/10.1073/pnas.0504136102

Fransson, P., Skiöld, B., Horsch, S., Nordell, A., Blennow, M., Lagercrantz, H., Åden, U., 2007. Resting-state networks in the infant brain. Proc. Natl. Acad. Sci. U.S.A. 104, 15531–15536. https://doi.org/10.1073/pnas.0704380104

Gao, W., Alcauter, S., Elton, A., Hernandez-Castillo, C.R., Smith, J.K., Ramirez, J., Lin, W., 2015a. Functional Network Development During the First Year: Relative Sequence and Socioeconomic Correlations. Cereb Cortex 25, 2919–2928. https://doi.org/10.1093/cercor/bhu088

Gao, W., Alcauter, S., Smith, J.K., Gilmore, J.H., Lin, W., 2015b. Development of human brain cortical network architecture during infancy. Brain Struct Funct 220, 1173–1186. https://doi.org/10.1007/s00429-014-0710-3

Gao, W., Elton, A., Zhu, H., Alcauter, S., Smith, J.K., Gilmore, J.H., Lin, W., 2014. Intersubject Variability of and Genetic Effects on the Brain's Functional Connectivity during Infancy. J. Neurosci. 34, 11288–11296. https://doi.org/10.1523/JNEUROSCI.5072-13.2014

Glasser, M.F., Sotiropoulos, S.N., Wilson, J.A., Coalson, T.S., Fischl, B., Andersson, J.L., Xu, J., Jbabdi, S., Webster, M., Polimeni, J.R., Van Essen, D.C., Jenkinson, M., 2013. The minimal preprocessing pipelines for the Human Connectome Project. NeuroImage, Mapping the Connectome 80, 105–124. https://doi.org/10.1016/j.neuroimage.2013.04.127

Gordon, E.M., Chauvin, R.J., Van, A.N., Rajesh, A., Nielsen, A., Newbold, D.J., Lynch, C.J., Seider, N.A., Krimmel, S.R., Scheidter, K.M., Monk, J., Miller, R.L., Metoki, A., Montez, D.F., Zheng, A., Elbau, I., Madison, T., Nishino, T., Myers, M.J., Kaplan, S., Badke D'Andrea, C., Demeter, D.V., Feigelis, M., Ramirez, J.S.B., Xu, T., Barch, D.M., Smyser, C.D., Rogers, C.E., Zimmermann, J., Botteron, K.N., Pruett, J.R., Willie, J.T., Brunner, P., Shimony, J.S., Kay, B.P., Marek, S., Norris, S.A., Gratton, C., Sylvester, C.M., Power,

J.D., Liston, C., Greene, D.J., Roland, J.L., Petersen, S.E., Raichle, M.E., Laumann, T.O., Fair, D.A., Dosenbach, N.U.F., 2023. A somato-cognitive action network alternates with effector regions in motor cortex. Nature 617. https://doi.org/10.1038/s41586-023-05964-2

Gordon, E.M., Laumann, T.O., Adeyemo, B., Gilmore, A.W., Nelson, S.M., Dosenbach, N.U.F., Petersen, S.E., 2017a. Individual-specific features of brain systems identified with resting state functional correlations. NeuroImage 146, 918–939. https://doi.org/10.1016/j.neuroimage.2016.08.032

Gordon, E.M., Laumann, T.O., Adeyemo, B., Huckins, J.F., Kelley, W.M., Petersen, S.E., 2016. Generation and Evaluation of a Cortical Area Parcellation from Resting-State Correlations. Cereb. Cortex 26, 288–303. https://doi.org/10.1093/cercor/bhu239

Gordon, E.M., Laumann, T.O., Adeyemo, B., Petersen, S.E., 2017b. Individual Variability of the System-Level Organization of the Human Brain. Cerebral Cortex 27, 386–399. https://doi.org/10.1093/cercor/bhv239

Gordon, E.M., Laumann, T.O., Gilmore, A.W., Newbold, D.J., Greene, D.J., Berg, J.J., Ortega, M., Hoyt-Drazen, C., Gratton, C., Sun, H., Hampton, J.M., Coalson, R.S., Nguyen, A.L., McDermott, K.B., Shimony, J.S., Snyder, A.Z., Schlaggar, B.L., Petersen, S.E., Nelson, S.M., Dosenbach, N.U.F., 2017c. Precision Functional Mapping of Individual Human Brains. Neuron 95. https://doi.org/10.1016/j.neuron.2017.07.011

Gordon, E.M., Laumann, T.O., Marek, S., Newbold, D.J., Hampton, J.M., Seider, N.A., Montez, D.F., Nielsen, A.M., Van, A.N., Zheng, A., Miller, R., Siegel, J.S., Kay, B.P., Snyder, A.Z., Greene, D.J., Schlaggar, B.L., Petersen, S.E., Nelson, S.M., Dosenbach, N.U.F., 2022. Individualized Functional Subnetworks Connect Human Striatum and Frontal Cortex. Cerebral Cortex 32, 2868–2884. https://doi.org/10.1093/cercor/bhab387

Gordon, E.M., Laumann, T.O., Marek, S., Raut, R.V., Gratton, C., Newbold, D.J., Greene, D.J., Coalson, R.S., Snyder, A.Z., Schlaggar, B.L., Petersen, S.E., Dosenbach, N.U.F., Nelson, S.M., 2020. Default-mode network streams for coupling to language and control systems. Proc Natl Acad Sci U S A 117, 17308–17319. https://doi.org/10.1073/pnas.2005238117

Gratton, C., Dworetsky, A., Adeyemo, B., Seitzman, B.A., Smith, D.M., Petersen, S.E., Neta, M., 2022. The cingulo-opercular network is composed of two distinct sub-systems (preprint). Neuroscience. https://doi.org/10.1101/2022.09.16.508254

Gratton, C., Laumann, T.O., Nielsen, A.N., Greene, D.J., Gordon, E.M., Gilmore, A.W., Nelson, S.M., Coalson, R.S., Snyder, A.Z., Schlaggar, B.L., Dosenbach, N.U.F., Petersen, S.E., 2018. Functional Brain Networks Are Dominated by Stable Group and Individual Factors, Not Cognitive or Daily Variation. Neuron 98, 439-452.e5. https://doi.org/10.1016/j.neuron.2018.03.035

Greicius, M.D., Krasnow, B., Reiss, A.L., Menon, V., 2003. Functional connectivity in the resting brain: A network analysis of the default mode hypothesis. Proc. Natl. Acad. Sci. U.S.A. 100, 253–258. https://doi.org/10.1073/pnas.0135058100

Hacker, C.D., Laumann, T.O., Szrama, N.P., Baldassarre, A., Snyder, A.Z., Leuthardt, E.C., Corbetta, M., 2013. Resting state network estimation in individual subjects. NeuroImage 82, 616–633. https://doi.org/10.1016/j.neuroimage.2013.05.108

Haxby, J.V., Guntupalli, J.S., Nastase, S.A., Feilong, M., 2020. Hyperalignment: Modeling shared information encoded in idiosyncratic cortical topographies. eLife 9, e56601. https://doi.org/10.7554/eLife.56601

Hermosillo, R.J.M., Moore, L.A., Feczko, E., Miranda-Domínguez, Ó., Pines, A., Dworetsky, A., Conan, G., Mooney, M.A., Randolph, A., Graham, A., Adeyemo, B., Earl, E., Perrone, A., Carrasco, C.M., Uriarte-Lopez, J., Snider, K., Doyle, O., Cordova, M., Koirala, S., Grimsrud, G.J., Byington, N., Nelson, S.M., Gratton, C., Petersen, S., Feldstein Ewing, S.W., Nagel, B.J., Dosenbach, N.U.F., Satterthwaite, T.D., Fair, D.A., 2024. A precision

functional atlas of personalized network topography and probabilities. Nat Neurosci 27, 1000–1013. https://doi.org/10.1038/s41593-024-01596-5

Hill, J., Dierker, D., Neil, J., Inder, T., Knutsen, A., Harwell, J., Coalson, T., Essen, D.V., 2010. A Surface-Based Analysis of Hemispheric Asymmetries and Folding of Cerebral Cortex in Term-Born Human Infants. J. Neurosci. 30, 2268–2276. https://doi.org/10.1523/JNEUROSCI.4682-09.2010

Holland, S.K., Vannest ,Jennifer, Mecoli ,Marc, Jacola ,Lisa M., Tillema ,Jan-Mendelt, Karunanayaka ,Prasanna R., Schmithorst ,Vincent J., Yuan ,Weihong, Plante ,Elena, and Byars, A.W., 2007. Functional MRI of language lateralization during development in children. International Journal of Audiology 46, 533–551. https://doi.org/10.1080/14992020701448994

Horovitz, S.G., Braun, A.R., Carr, W.S., Picchioni, D., Balkin, T.J., Fukunaga, M., Duyn, J.H., 2009. Decoupling of the brain's default mode network during deep sleep. Proceedings of the National Academy of Sciences 106, 11376–11381. https://doi.org/10.1073/pnas.0901435106

Howell, B.R., Styner, M.A., Gao, W., Yap, P.-T., Wang, L., Baluyot, K., Yacoub, E., Chen, G., Potts, T., Salzwedel, A., Li, G., Gilmore, J.H., Piven, J., Smith, J.K., Shen, D., Ugurbil, K., Zhu, H., Lin, W., Elison, J.T., 2019. The UNC/UMN Baby Connectome Project (BCP): An overview of the study design and protocol development. NeuroImage 185, 891–905. https://doi.org/10.1016/j.neuroimage.2018.03.049

Huth, A.G., de Heer, W.A., Griffiths, T.L., Theunissen, F.E., Gallant, J.L., 2016. Natural speech reveals the semantic maps that tile human cerebral cortex. Nature 532, 453–458. https://doi.org/10.1038/nature17637

Ji, J.L., Spronk, M., Kulkarni, K., Repovš, G., Anticevic, A., Cole, M.W., 2019. Mapping the human brain's cortical-subcortical functional network organization. NeuroImage 185, 35–57. https://doi.org/10.1016/j.neuroimage.2018.10.006

Kaplan, S., Meyer, D., Miranda-Dominguez, O., Perrone, A., Earl, E., Alexopoulos, D., Barch, D.M., Day, T.K.M., Dust, J., Eggebrecht, A.T., Feczko, E., Kardan, O., Kenley, J.K., Rogers, C.E., Wheelock, M.D., Yacoub, E., Rosenberg, M., Elison, J.T., Fair, D.A., Smyser, C.D., 2022. Filtering respiratory motion artifact from resting state fMRI data in infant and toddler populations. NeuroImage 247, 118838. https://doi.org/10.1016/j.neuroimage.2021.118838

Kardan, O., Kaplan, S., Wheelock, M.D., Feczko, E., Day, T.K.M., Miranda-Domínguez, Ó., Meyer, D., Eggebrecht, A.T., Moore, L.A., Sung, S., Chamberlain, T.A., Earl, E., Snider, K., Graham, A., Berman, M.G., Uğurbil, K., Yacoub, E., Elison, J.T., Smyser, C.D., Fair, D.A., Rosenberg, M.D., 2022. Resting-state functional connectivity identifies individuals and predicts age in 8-to-26-month-olds. Developmental Cognitive Neuroscience 56, 101123. https://doi.org/10.1016/j.dcn.2022.101123

Kong, R., Li, J., Orban, C., Sabuncu, M.R., Liu, H., Schaefer, A., Sun, N., Zuo, X.-N., Holmes, A.J., Eickhoff, S.B., Yeo, B.T.T., 2019. Spatial Topography of Individual-Specific Cortical Networks Predicts Human Cognition, Personality, and Emotion. Cerebral Cortex 29, 2533–2551. https://doi.org/10.1093/cercor/bhy123

Kong, R., Spreng, R.N., Xue, A., Betzel, R.F., Cohen, J.R., Damoiseaux, J.S., De Brigard, F., Eickhoff, S.B., Fornito, A., Gratton, C., Gordon, E.M., Holmes, A.J., Laird, A.R., Larson-Prior, L., Nickerson, L.D., Pinho, A.L., Razi, A., Sadaghiani, S., Shine, J.M., Yendiki, A., Yeo, B.T.T., Uddin, L.Q., 2025. A network correspondence toolbox for quantitative evaluation of novel neuroimaging results. Nat Commun 16, 2930. https://doi.org/10.1038/s41467-025-58176-9

Koyama, M.S., O'Connor, D., Shehzad, Z., Milham, M.P., 2017. Differential contributions of the middle frontal gyrus functional connectivity to literacy and numeracy. Sci Rep 7, 17548. https://doi.org/10.1038/s41598-017-17702-6

Kraus, B.T., Perez, D., Ladwig, Z., Seitzman, B.A., Dworetsky, A., Petersen, S.E., Gratton, C., 2021. Network variants are similar between task and rest states. NeuroImage 229, 117743. https://doi.org/10.1016/j.neuroimage.2021.117743

Kwon, Y.H., Salvo, J.J., Anderson, N.L., Edmonds, D., Holubecki, A.M., Lakshman, M., Yoo, K., Yeo, B.T.T., Kay, K., Gratton, C., Braga, R.M., 2025. Situating the salience and parietal memory networks in the context of multiple parallel distributed networks using precision functional mapping. Cell Reports 44. https://doi.org/10.1016/j.celrep.2024.115207

Ladwig, Z., Kermani, K.Z., Dworetsky, A., Labora, N., Hernandez, J.J., Dorn, M., Smith, D.M., Nee, D.E., Petersen, S.E., Braga, R.M., Gratton, C., 2025. Precision fMRI reveals densely interdigitated network patches with conserved motifs in the lateral prefrontal cortex. https://doi.org/10.1101/2025.07.24.666468

Lange, T., Roth, V., Braun, M.L., Buhmann, J.M., 2004. Stability-Based Validation of Clustering Solutions. Neural Computation 16, 1299–1323. https://doi.org/10.1162/089976604773717621

Langs, G., Wang, D., Golland, P., Mueller, S., Pan, R., Sabuncu, M.R., Sun, W., Li, K., Liu, H., 2016. Identifying Shared Brain Networks in Individuals by Decoupling Functional and Anatomical Variability. Cerebral Cortex 26, 4004–4014. https://doi.org/10.1093/cercor/bhv189

Larson-Prior, L.J., Power, J.D., Vincent, J.L., Nolan, T.S., Coalson, R.S., Zempel, J., Snyder, A.Z., Schlaggar, B.L., Raichle, M.E., Petersen, S.E., 2011. Chapter 18 - Modulation of the brain's functional network architecture in the transition from wake to sleep, in: Van Someren, E.J.W., Van Der Werf, Y.D., Roelfsema, P.R., Mansvelder, H.D., Lopes Da Silva, F.H. (Eds.), Progress in Brain Research, Slow Brain Oscillations of Sleep, Resting State and Vigilance. Elsevier, pp. 277–294. https://doi.org/10.1016/B978-0-444-53839-0.00018-1

Larson-Prior, L.J., Zempel, J.M., Nolan, T.S., Prior, F.W., Snyder, A.Z., Raichle, M.E., 2009. Cortical network functional connectivity in the descent to sleep. Proceedings of the National Academy of Sciences 106, 4489–4494. https://doi.org/10.1073/pnas.0900924106

Laumann, T.O., Gordon, E.M., Adeyemo, B., Snyder, A.Z., Joo, S.J., Chen, M.-Y., Gilmore, A.W., McDermott, K.B., Nelson, S.M., Dosenbach, N.U.F., Schlaggar, B.L., Mumford, J.A., Poldrack, R.A., Petersen, S.E., 2015. Functional System and Areal Organization of a Highly Sampled Individual Human Brain. Neuron 87, 657–670. https://doi.org/10.1016/j.neuron.2015.06.037

Li, M., Wang, D., Ren, J., Langs, G., Stoecklein, S., Brennan, B.P., Lu, J., Chen, H., Liu, H., 2019. Performing group-level functional image analyses based on homologous functional regions mapped in individuals. PLOS Biology 17, e2007032. https://doi.org/10.1371/journal.pbio.2007032

Lidzba, K., Schwilling, E., Grodd, W., Krägeloh-Mann, I., Wilke, M., 2011. Language comprehension vs. language production: Age effects on fMRI activation. Brain and Language 119, 6–15. https://doi.org/10.1016/j.bandl.2011.02.003

Lipkin, B., Tuckute, G., Affourtit, J., Small, H., Mineroff, Z., Kean, H., Jouravlev, O., Rakocevic, L., Pritchett, B., Siegelman, M., Hoeflin, C., Pongos, A., Blank, I.A., Struhl, M.K., Ivanova, A., Shannon, S., Sathe, A., Hoffmann, M., Nieto-Castañón, A., Fedorenko, E., 2022. Probabilistic atlas for the language network based on precision fMRI data from >800 individuals. Sci Data 9, 529. https://doi.org/10.1038/s41597-022-01645-3

Luckett, P.H., Lee, J.J., Park, K.Y., Raut, R.V., Meeker, K.L., Gordon, E.M., Snyder, A.Z., Ances, B.M., Leuthardt, E.C., Shimony, J.S., 2023. Resting state network mapping in individuals using deep learning. Frontiers in Neurology 13.

Lynch, C.J., Elbau, I.G., Ng, T., Ayaz, A., Zhu, S., Wolk, D., Manfredi, N., Johnson, M., Chang, M., Chou, J., Summerville, I., Ho, C., Lueckel, M., Bukhari, H., Buchanan, D., Victoria,

L.W., Solomonov, N., Goldwaser, E., Moia, S., Caballero-Gaudes, C., Downar, J., Vila-Rodriguez, F., Daskalakis, Z.J., Blumberger, D.M., Kay, K., Aloysi, A., Gordon, E.M., Bhati, M.T., Williams, N., Power, J.D., Zebley, B., Grosenick, L., Gunning, F.M., Liston, C., 2024. Frontostriatal salience network expansion in individuals in depression. Nature 633, 624–633. https://doi.org/10.1038/s41586-024-07805-2

Lynch, C.J., Elbau, I.G., Ng, T.H., Wolk, D., Zhu, S., Ayaz, A., Power, J.D., Zebley, B., Gunning, F.M., Liston, C., 2022. Automated optimization of TMS coil placement for personalized functional network engagement. Neuron 110, 3263-3277.e4. https://doi.org/10.1016/j.neuron.2022.08.012

Marrus, N., Eggebrecht, A.T., Todorov, A., Elison, J.T., Wolff, J.J., Cole, L., Gao, W., Pandey, J., Shen, M.D., Swanson, M.R., Emerson, R.W., Klohr, C.L., Adams, C.M., Estes, A.M., Zwaigenbaum, L., Botteron, K.N., McKinstry, R.C., Constantino, J.N., Evans, A.C., Hazlett, H.C., Dager, S.R., Paterson, S.J., Schultz, R.T., Styner, M.A., Gerig, G., The IBIS Network, Schlaggar, B.L., Piven, J., Pruett, J.R., Jr., 2018. Walking, Gross Motor Development, and Brain Functional Connectivity in Infants and Toddlers. Cerebral Cortex 28, 750–763. https://doi.org/10.1093/cercor/bhx313

Meschke, E.X., Castello, M.V.D.O., Tour, T.D.L., Gallant, J.L., 2023. Model connectivity: leveraging the power of encoding models to overcome the limitations of functional connectivity. https://doi.org/10.1101/2023.07.17.549356

Miranda-Dominguez, O., Mills, B.D., Carpenter, S.D., Grant, K.A., Kroenke, C.D., Nigg, J.T., Fair, D.A., 2014. Connectotyping: Model Based Fingerprinting of the Functional Connectome. PLOS ONE 9, e111048. https://doi.org/10.1371/journal.pone.0111048

Mitra, A., Snyder, A.Z., Tagliazucchi, E., Laufs, H., Raichle, M.E., 2015. Propagated infra-slow intrinsic brain activity reorganizes across wake and slow wave sleep. eLife 4, e10781. https://doi.org/10.7554/eLife.10781

Molloy, M.F., Saygin, Z.M., 2022. Individual variability in functional organization of the neonatal brain. NeuroImage 253, 119101. https://doi.org/10.1016/j.neuroimage.2022.119101

Moore, L.A., Hermosillo, R.J.M., Feczko, E., Moser, J., Koirala, S., Allen, M.C., Buss, C., Conan, G., Juliano, A.C., Marr, M., Miranda-Dominguez, O., Mooney, M., Myers, M., Rasmussen, J., Rogers, C.E., Smyser, C.D., Snider, K., Sylvester, C., Thomas, E., Fair, D.A., Graham, A.M., 2024. Towards personalized precision functional mapping in infancy. Imaging Neuroscience 2, 1–20. https://doi.org/10.1162/imag_a_00165

Moser, J., Nelson, S.M., Koirala, S., Madison, T.J., Labonte, A.K., Carrasco, C.M., Feczko, E., Moore, L.A., Lundquist, J.T., Weldon, K.B., Grimsrud, G., Hufnagle, K., Ahmed, W., Myers, M.J., Adeyemo, B., Snyder, A.Z., Gordon, E.M., Dosenbach, N.U.F., Tervo-Clemmens, B., Larsen, B., Moeller, S., Yacoub, E., Vizioli, L., Uğurbil, K., Laumann, T.O., Sylvester, C.M., Fair, D.A., 2025. Multi-echo acquisition and thermal denoising advances precision functional imaging. Imaging Neuroscience 3, imag_a_00426. https://doi.org/10.1162/imag_a_00426

Mueller, S., Wang, D., Fox, M.D., Yeo, B.T.T., Sepulcre, J., Sabuncu, M.R., Shafee, R., Lu, J., Liu, H., 2013. Individual Variability in Functional Connectivity Architecture of the Human Brain. Neuron 77, 586–595. https://doi.org/10.1016/j.neuron.2012.12.028

Mullen, E.M., 1995. Mullen scales of early learning. AGS Circle Pines, MN.

Myers, M.J., Labonte, A.K., Gordon, E.M., Laumann, T.O., Tu, J.C., Wheelock, M.D., Nielsen, A.N., Schwarzlose, R.F., Camacho, M.C., Alexopoulos, D., Warner, B.B., Raghuraman, N., Luby, J.L., Barch, D.M., Fair, D.A., Petersen, S.E., Rogers, C.E., Smyser, C.D., Sylvester, C.M., 2024. Functional parcellation of the neonatal cortical surface. Cerebral Cortex 34, bhae047. https://doi.org/10.1093/cercor/bhae047

Myoraku, A., Lang, A., Taylor, C.T., Scott Mackin, R., Meyerhoff, D.J., Mueller, S., Strigo, I.A., Tosun, D., 2022. Age-dependent brain morphometry in Major Depressive disorder. NeuroImage: Clinical 33, 102924. https://doi.org/10.1016/j.nicl.2021.102924

Nahas, Z., Fair, D., Netoff, T., Darrow, D., Park, M., Hermosillo, R., Eiting, S., Koenig, S., Herman, A., Widge, A., Hazimeh, M., Durrani, B., Chaikind, J., Johnson, R., 2025. Prefrontal Cortical Stimulation for Treatment-Resistant Depression. Brain Stimulation: Basic, Translational, and Clinical Research in Neuromodulation 18, 1334. https://doi.org/10.1016/j.brs.2025.05.016

Newbold, D.J., Laumann, T.O., Hoyt, C.R., Hampton, J.M., Montez, D.F., Raut, R.V., Ortega, M., Mitra, A., Nielsen, A.N., Miller, D.B., Adeyemo, B., Nguyen, A.L., Scheidter, K.M., Tanenbaum, A.B., Van, A.N., Marek, S., Schlaggar, B.L., Carter, A.R., Greene, D.J., Gordon, E.M., Raichle, M.E., Petersen, S.E., Snyder, A.Z., Dosenbach, N.U.F., 2020. Plasticity and Spontaneous Activity Pulses in Disused Human Brain Circuits. Neuron 107, 580-589.e6. https://doi.org/10.1016/j.neuron.2020.05.007

Nielsen, A.N., Graham, A.M., Sylvester, C.M., 2023. Baby Brains at Work: How Task-Based Functional Magnetic Resonance Imaging Can Illuminate the Early Emergence of Psychiatric Risk. Biological Psychiatry, The Infant Brain: A Critical Antecedent of Psychiatric Risk 93, 880–892. https://doi.org/10.1016/j.biopsych.2023.01.010

Nomi, J.S., Farrant, K., Damaraju, E., Rachakonda, S., Calhoun, V.D., Uddin, L.Q., 2016. Dynamic functional network connectivity reveals unique and overlapping profiles of insula subdivisions. Human Brain Mapping 37, 1770–1787. https://doi.org/10.1002/hbm.23135

Olulade, O.A., Seydell-Greenwald, A., Chambers, C.E., Turkeltaub, P.E., Dromerick, A.W., Berl, M.M., Gaillard, W.D., Newport, E.L., 2020. The neural basis of language development: Changes in lateralization over age. Proceedings of the National Academy of Sciences 117, 23477–23483. https://doi.org/10.1073/pnas.1905590117

Ooi, L.Q.R., Orban, C., Zhang, S., Nichols, T.E., Tan, T.W.K., Kong, R., Marek, S., Dosenbach, N.U.F., Laumann, T.O., Gordon, E.M., Yap, K.H., Ji, F., Chong, J.S.X., Chen, C., An, L., Franzmeier, N., Roemer-Cassiano, S.N., Hu, Q., Ren, J., Liu, H., Chopra, S., Cocuzza, C.V., Baker, J.T., Zhou, J.H., Bzdok, D., Eickhoff, S.B., Holmes, A.J., Yeo, B.T.T., 2025. Longer scans boost prediction and cut costs in brain-wide association studies. Nature 1–10. https://doi.org/10.1038/s41586-025-09250-1

Palomero-Gallagher, N., Hoffstaedter, F., Mohlberg, H., Eickhoff, S.B., Amunts, K., Zilles, K., 2019. Human Pregenual Anterior Cingulate Cortex: Structural, Functional, and Connectional Heterogeneity. Cereb Cortex 29, 2552–2574. https://doi.org/10.1093/cercor/bhy124

Paquola, C., Garber, M., Frässle, S., Royer, J., Zhou, Y., Tavakol, S., Rodriguez-Cruces, R., Cabalo, D.G., Valk, S., Eickhoff, S.B., Margulies, D.S., Evans, A., Amunts, K., Jefferies, E., Smallwood, J., Bernhardt, B.C., 2025. The architecture of the human default mode network explored through cytoarchitecture, wiring and signal flow. Nat Neurosci 28, 654–664. https://doi.org/10.1038/s41593-024-01868-0

Perez, D.C., Dworetsky, A., Braga, R.M., Beeman, M., Gratton, C., 2023. Hemispheric Asymmetries of Individual Differences in Functional Connectivity. J Cogn Neurosci 35, 200–225. https://doi.org/10.1162/jocn_a_01945

Power, J.D., Cohen, A.L., Nelson, S.M., Wig, G.S., Barnes, K.A., Church, J.A., Vogel, A.C., Laumann, T.O., Miezin, F.M., Schlaggar, B.L., Petersen, S.E., 2011. Functional Network Organization of the Human Brain. Neuron 72, 665–678. https://doi.org/10.1016/j.neuron.2011.09.006

Power, J.D., Mitra, A., Laumann, T.O., Snyder, A.Z., Schlaggar, B.L., Petersen, S.E., 2014. Methods to detect, characterize, and remove motion artifact in resting state fMRI. NeuroImage 84, 320–341. https://doi.org/10.1016/j.neuroimage.2013.08.048

Rai, S., Godfrey, K.J., Graff, K., Tansey, R., Merrikh, D., Yin, S., Feigelis, M., Demeter, D.V., Vanderwal, T., Greene, D.J., Bray, S., 2025. How much is “enough”? Considerations for

functional connectivity reliability in pediatric naturalistic fMRI. Imaging Neuroscience 3, IMAG.a.117. https://doi.org/10.1162/IMAG.a.117

Roffwarg, H.P., Muzio, J.N., Dement, W.C., 1966. Ontogenetic Development of the Human Sleep-Dream Cycle. Science 152, 604–619. https://doi.org/10.1126/science.152.3722.604

Rousseeuw, P.J., 1987. Silhouettes: A graphical aid to the interpretation and validation of cluster analysis. Journal of Computational and Applied Mathematics 20, 53–65. https://doi.org/10.1016/0377-0427(87)90125-7

Rubinov, M., Sporns, O., 2011. Weight-conserving characterization of complex functional brain networks. NeuroImage 56, 2068–2079. https://doi.org/10.1016/j.neuroimage.2011.03.069

Salo, T., Yarkoni, T., Nichols, T.E., Poline, J.-B., Bilgel, M., Bottenhorn, K.L., Jarecka, D., Kent, J.D., Kimbler, A., Nielson, D.M., Oudyk, K.M., Peraza, J.A., Pérez, A., Reeders, P.C., Yanes, J.A., Laird, A.R., 2023. NiMARE: Neuroimaging Meta-Analysis Research Environment. Aperture Neuro 3, 1–32. https://doi.org/10.52294/001c.87681

Seitzman, B.A., Gratton, C., Laumann, T.O., Gordon, E.M., Adeyemo, B., Dworetsky, A., Kraus, B.T., Gilmore, A.W., Berg, J.J., Ortega, M., Nguyen, A., Greene, D.J., McDermott, K.B., Nelson, S.M., Lessov-Schlaggar, C.N., Schlaggar, B.L., Dosenbach, N.U.F., Petersen, S.E., 2019. Trait-like variants in human functional brain networks. Proc. Natl. Acad. Sci. U.S.A. 116, 22851–22861. https://doi.org/10.1073/pnas.1902932116

Seitzman, B.A., Gratton, C., Marek, S., Raut, R.V., Dosenbach, N.U.F., Schlaggar, B.L., Petersen, S.E., Greene, D.J., 2020. A set of functionally-defined brain regions with improved representation of the subcortex and cerebellum. NeuroImage 206, 116290. https://doi.org/10.1016/j.neuroimage.2019.116290

Sepeta, L.N., Berl, M.M., Wilke, M., You, X., Mehta, M., Xu, B., Inati, S., Dustin, I., Khan, O., Austermuehle, A., Theodore, W.H., Gaillard, W.D., 2016. Age-dependent mesial temporal lobe lateralization in language fMRI. Epilepsia 57, 122–130. https://doi.org/10.1111/epi.13258

Shen, X., Tokoglu, F., Papademetris, X., Constable, R.T., 2013. Groupwise whole-brain parcellation from resting-state fMRI data for network node identification. NeuroImage 82, 403–415. https://doi.org/10.1016/j.neuroimage.2013.05.081

Shinn, M., Romero-Garcia, R., Seidlitz, J., Váša, F., Vértes, P.E., Bullmore, E., 2017. Versatility of nodal affiliation to communities. Sci Rep 7, 4273. https://doi.org/10.1038/s41598-017-03394-5

Stephens, R.L., Langworthy, B., Short, S.J., Goldman, B.D., Girault, J.B., Fine, J.P., Reznick, J.S., Gilmore, J.H., 2018. Verbal and nonverbal predictors of executive function in early childhood. J Cogn Dev 19, 182–200. https://doi.org/10.1080/15248372.2018.1439493

Sun, L., Zhao, T., Liang, X., Xia, M., Li, Q., Liao, X., Gong, G., Wang, Q., Pang, C., Yu, Q., Bi, Y., Chen, P., Chen, R., Chen, Y., Chen, T., Cheng, J., Cheng, Y., Cui, Z., Dai, Z., Deng, Y., Ding, Y., Dong, Q., Duan, D., Gao, J.-H., Gong, Q., Han, Y., Han, Z., Huang, C.-C., Huang, R., Huo, R., Li, L., Lin, C.-P., Lin, Q., Liu, B., Liu, C., Liu, N., Liu, Ying, Liu, Yong, Lu, J., Ma, L., Men, W., Qin, S., Qiu, J., Qiu, S., Si, T., Tan, S., Tang, Y., Tao, S., Wang, D., Wang, F., Wang, J., Wang, P., Wang, X., Wang, Y., Wei, D., Wu, Y., Xie, P., Xu, X., Xu, Y., Xu, Z., Yang, L., Yuan, H., Zeng, Z., Zhang, H., Zhang, X., Zhao, G., Zheng, Y., Zhong, S., He, Y., 2025. Human lifespan changes in the brain's functional connectome. Nat Neurosci 28, 891–901. https://doi.org/10.1038/s41593-025-01907-4

Sylvester, C.M., Kaplan, S., Myers, M.J., Gordon, E.M., Schwarzlose, R.F., Alexopoulos, D., Nielsen, A.N., Kenley, J.K., Meyer, D., Yu, Q., Graham, A.M., Fair, D.A., Warner, B.B., Barch, D.M., Rogers, C.E., Luby, J.L., Petersen, S.E., Smyser, C.D., 2022. Network-specific selectivity of functional connections in the neonatal brain. Cerebral Cortex bhac202. https://doi.org/10.1093/cercor/bhac202

Szaflarski, J.P., Holland, S.K., Schmithorst, V.J., Byars, A.W., 2006a. fMRI study of language lateralization in children and adults. Human Brain Mapping 27, 202–212. https://doi.org/10.1002/hbm.20177

Szaflarski, J.P., Schmithorst, V.J., Altaye, M., Byars, A.W., Ret, J., Plante, E., Holland, S.K., 2006b. A longitudinal functional magnetic resonance imaging study of language development in children 5 to 11 years old. Annals of Neurology 59, 796–807. https://doi.org/10.1002/ana.20817

Tagliazucchi, E., von Wegner, F., Morzelewski, A., Borisov, S., Jahnke, K., Laufs, H., 2012. Automatic sleep staging using fMRI functional connectivity data. NeuroImage 63, 63–72. https://doi.org/10.1016/j.neuroimage.2012.06.036

Tagliazucchi, E., von Wegner, F., Morzelewski, A., Brodbeck, V., Jahnke, K., Laufs, H., 2013. Breakdown of long-range temporal dependence in default mode and attention networks during deep sleep. Proc. Natl. Acad. Sci. U.S.A. 110, 15419–15424. https://doi.org/10.1073/pnas.1312848110

Tooley, U.A., Latham, A., Kenley, J.K., Alexopoulos, D., Smyser, T.A., Nielsen, A.N., Gorham, L., Warner, B.B., Shimony, J.S., Neil, J.J., 2024. Prenatal environment is associated with the pace of cortical network development over the first three years of life. Nature Communications 15, 7932.

Tu, J.C., Myers, M.J., Li, W., Li, J., Wang, X., Dierker, D., Day, T.K.M., Snyder, A., Latham, A., Kenley, J.K., Sobolewski, C.M., Wang, Y., Labonte, A.K., Feczko, E., Kardan, O., Moore, L.A., Sylvester, C.M., Fair, D.A., Elison, J.T., Warner, B.B., Barch, D.M., Rogers, C.E., Luby, J.L., Smyser, C.D., Gordon, E.M., Laumann, T.O., Eggebrecht, A.T., Wheelock, M.D., 2025a. The generalizability of cortical area parcellations across early childhood. Cerebral Cortex 35, bhaf116. https://doi.org/10.1093/cercor/bhaf116

Tu, J.C., Wang, Y., Wang, X., Dierker, D., Sobolewski, C.M., Day, T.K.M., Kardan, O., Miranda-Domínguez, Ó., Moore, L.A., Feczko, E., Fair, D.A., Elison, J.T., Gordon, E.M., Laumann, T.O., Eggebrecht, A.T., Wheelock, M.D., 2025b. A subset of cortical areas exhibit adult-like functional network patterns in early childhood. Developmental Cognitive Neuroscience 73, 101551. https://doi.org/10.1016/j.dcn.2025.101551

Uddin, L.Q., Clare Kelly, A. m., Biswal, B.B., Xavier Castellanos, F., Milham, M.P., 2009. Functional connectivity of default mode network components: Correlation, anticorrelation, and causality. Human Brain Mapping 30, 625–637. https://doi.org/10.1002/hbm.20531

Van Essen, D.C., Glasser, M.F., Dierker, D.L., Harwell, J., Coalson, T., 2012. Parcellations and Hemispheric Asymmetries of Human Cerebral Cortex Analyzed on Surface-Based Atlases. Cerebral Cortex 22, 2241–2262. https://doi.org/10.1093/cercor/bhr291

Wang, D., Buckner, R.L., Fox, M.D., Holt, D.J., Holmes, A.J., Stoecklein, S., Langs, G., Pan, R., Qian, T., Li, K., Baker, J.T., Stufflebeam, S.M., Wang, K., Wang, X., Hong, B., Liu, H., 2015. Parcellating cortical functional networks in individuals. Nat Neurosci 18, 1853–1860. https://doi.org/10.1038/nn.4164

Wang, D., Buckner, R.L., Liu, H., 2014. Functional Specialization in the Human Brain Estimated By Intrinsic Hemispheric Interaction. J. Neurosci. 34, 12341–12352. https://doi.org/10.1523/JNEUROSCI.0787-14.2014

Wang, F., Zhang, H., Wu, Z., Hu, D., Zhou, Z., Girault, J.B., Wang, L., Lin, W., Li, G., 2023. Fine-grained functional parcellation maps of the infant cerebral cortex. eLife 12, e75401. https://doi.org/10.7554/eLife.75401

Xu, Y., Cao, M., Liao, X., Xia, M., Wang, X., Jeon, T., Ouyang, M., Chalak, L., Rollins, N., Huang, H., He, Y., 2019. Development and Emergence of Individual Variability in the Functional Connectivity Architecture of the Preterm Human Brain. Cerebral Cortex 29, 4208–4222. https://doi.org/10.1093/cercor/bhy302

Yang, F.N., Picchioni, D., Zwart, J.A. de, Wang, Y., Gelderen, P. van, Duyn, J.H., 2024. Reproducible, data-driven characterization of sleep based on brain dynamics and transitions from whole-night fMRI [WWW Document]. eLife. https://doi.org/10.7554/eLife.98739

Yeo, B.T.T., Krienen, F.M., Sepulcre, J., Sabuncu, M.R., Lashkari, D., Hollinshead, M., Roffman, J.L., Smoller, J.W., Zöllei, L., Polimeni, J.R., Fischl, B., Liu, H., Buckner, R.L., 2011. The organization of the human cerebral cortex estimated by intrinsic functional connectivity. Journal of Neurophysiology 106, 1125–1165. https://doi.org/10.1152/jn.00338.2011

Zhang, X.-H., Anderson, K.M., Dong, H.-M., Chopra, S., Dhamala, E., Emani, P.S., Gerstein, M.B., Margulies, D.S., Holmes, A.J., 2024. The cell-type underpinnings of the human functional cortical connectome. Nat Neurosci 1–11. https://doi.org/10.1038/s41593-024-01812-2

Zhi, D., King, M., Hernandez-Castillo, C.R., Diedrichsen, J., 2022. Evaluating brain parcellations using the distance-controlled boundary coefficient. Human Brain Mapping 43, 3706–3720. https://doi.org/10.1002/hbm.25878

Zhu, Z., Yang, H., Wen, H., Hung, J., Hu, Y., Bi, Y., Yu, X., 2025. Innate network mechanisms of temporal pole for semantic cognition in neonatal and adult twin studies. Nat Commun 16, 3835. https://doi.org/10.1038/s41467-025-58896-y